Univerzita Karlova v Praze
Matematicko-fyzikální fakulta

DIPLOMOVÁ PRÁCE

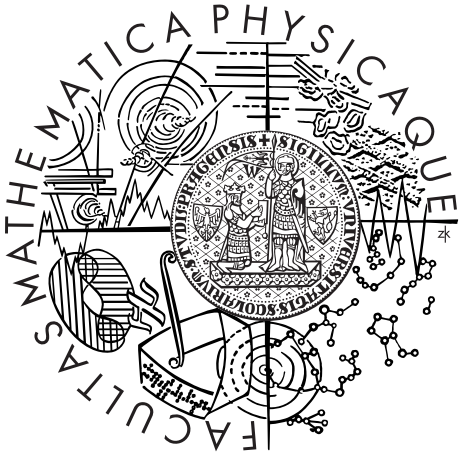

Ondřej Krejčí

Teoretické výpočty interakce adsorbátu s orientovanými povrchy Si

Katedra fyziky povrchů a plazmatu

Vedoucí diplomové práce: RNDr. Pavel Kocán, Ph.D.

Studijní program: Fyzika

Studijní obor: Biofyzika a chemická fyzika

Praha ROK 2013

Charles University in Prague
Faculty of Mathematics and Physics

MASTER THESIS

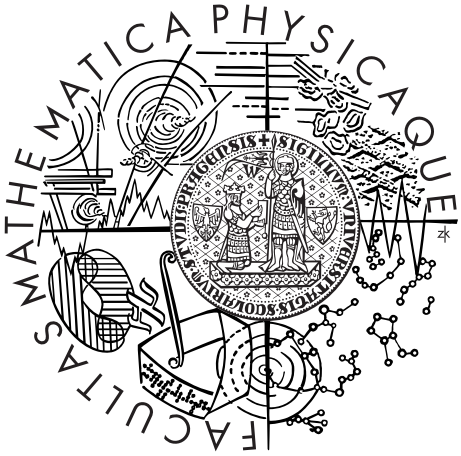

Ondřej Krejčí

Theoretical calculation of interaction between adsorbate and oriented Si surfaces

Department of Surface and Plasma Science

Supervisor of the master thesis: RNDr. Pavel Kocán, Ph.D.

Study programme: Physics

Specialization: Biophysics and Chemical Physics

Prague YEAR 2013

On this place I would like to thank to my supervisor RNDr. Pavel Kocán, Ph.D for inviting me into field of surface science and nanoscience. I also would like to thank him for his help with this work, for the uneasy questions that forced me to improve myself and for interesting experimental observations, that I could support with my calculations.

I want to express my sincere gratitude to Ing. Pavel Jelínek, Ph.D. for opening the door of computational physics to me and for his support in my beginnings. I also want to thank him for the opportunity to work in his group, for provision of computational codes Fireball and STM and for his help with this work.

I am grateful to all members of nanosurf group who helped me with my calculations and who supports me with their deep knowledge. Especially I want to thank to Dr. Ing. Pingo Mutombo for his help with STM simulations.

I also want to thank to Prof. Alastair McLean for the opportunity to support his experimental work with my calculations and for the the last corrections of this work.

I would like to express my appreciation to my friend Lucie Mornsteinová who helped me with the corrections.

I would like to thank to FZÚ, AV ČR, v.v.i. for providing the Dorje and David computational clusters, on which the calculations for this work were made.

I declare that I carried out this master thesis independently, and only with the cited sources, literature and other professional sources.

I understand that my work relates to the rights and obligations under the Act No. 121/2000 Coll., the Copyright Act, as amended, in particular the fact that the Charles University in Prague has the right to conclude a license agreement on the use of this work as a school work pursuant to Section 60 paragraph 1 of the Copyright Act.

In ..... date ..... signature of the author

Název práce: Teoretické výpočty interakce adsorbátu s orientovanými povrchy Si

Autor: Ondřej Krejčí

Katedra: Katedra fyziky povrchů a plazmatu

Vedoucí diplomové práce: RNDr. Pavel Kocán, Ph.D., Katedra fyziky povrchů a plazmatu

Konultant diplomové práce: Ing. Pavel Jelínek, Ph.D., Fyzikální ústav AV ČR, v.v.i., Sekce fyziky pevných látek, Oddělení tenkých vrstev a nanostruktur

Abstrakt: V této práci jsem stručně popsal základy metody funkcionálu hustoty (DFT) pro výpočet elektronové struktury molekul, pevných látek a povrchů. Dále, jsem zde shrnul základní stavební kameny výpočetního programu Fireball, který využívá metody DFT a se kterým jsem následně prováděl výpočty atomární a elektronové struktury vybraných modelů. Také jsem se zabýval teorií skenovací tunelovací mikroskopie (STM) a přístupy jak simulovat STM mapy na základě DFT výpočtů. Studovanými modely byly rekonstrukce povrchu Si (111), konkrétně šlo o rekonstrukce 7×7, 2×1 *Pandey chain.* a dále pak rekonstrukce s periodicitou $\sqrt{3}\times\sqrt{3}$, kde bylo úkolem nalezení vhodné atomární struktury, odpovídající novým experimentálním poznatkům. Následně jsem provedl porovnání energetické výhodnosti jednotlivých rekonstrukcí. Posledním studovaným modelem byla adsorpce molekuly benzenu na nejstabilnější rekonstrukci 7×7. U všech modelů jsem provedl analýzu atomární a elektronové struktury a pomocí kódu STM jsem simuloval jejich STM mapy. Ty jsem následně porovnal s experimentálními STM měřeními v literatuře a s výsledky experimentů, které prováděli RNDr. Pavel Kocán, Ph.D. (rekonstrukce $\sqrt{3}\times\sqrt{3}$) a Prof. Alastair McLean (benzen na 7×7). Byl nalezen pravděpodobný model pozorované metastabilní rekonstrukce $\sqrt{3}\times\sqrt{3}$. Také byla prokázána chemisorpce benzenu v takzvané di-σ-můstkové konfiguraci.

Klíčová slova: DFT, STM, rekonstrukce povrchů, adsorpce.

Title: Theoretical calculation of interaction between adsorbate and oriented Si surfaces

Author: Ondřej Krejčí

Department: Department of Surface and Plasma Science

Supervisor: RNDr. Pavel Kocán, Ph.D., Department of Surface and Plasma Science

Tutor: Ing. Pavel Jelínek, Ph.D., Institute of physics of the AS CR, v.v.i., Division of Solid State Physics, Department of Thin Films and Nanostructures

Abstract: In this work I briefly described the basic ideas of density functional theory (DFT) for calculations of an electronic structure of molecules, solids and surfaces. I also summarized the fundamentals of DFT based Fireball code that was used for calculations of the atomic and electronic structures of several models. Further I described theory of scanning tunnelling microscopy (STM) and mentioned some approaches of simulating STM maps by means of results of DFT calculations. The studied models were reconstructions of a Si (111) surface, namely the 7×7, 2×1 *Pandey chain* and reconstructions with periodicity $\sqrt{3}\times\sqrt{3}$, where finding proper atomic structure, fitting to a new experimental observations, was required. I compared energetic favourableness of the reconstructions. I also studied an adsorption of benzene on 7×7. I have analysed the atomic and electronic structure of all the models and made STM simulations using STM code. I compared the results with experimental STM maps in literature and with results of the STM experiments made by RNDr. Pavel Kocán, Ph.D. (reconstruction v$\sqrt{3}\times\sqrt{3}$) and by Prof. Alastair McLean (benzene on 7×7). Probable model of observed metastable reconstruction $\sqrt{3}\times\sqrt{3}$ was found. The proof that benzene chamisorbate in so called di-σ-bridge position was also made.

Keywords: DFT, STM, reconstruction of surfaces, adsorption.

Contents

Introduction

All of the computing technology nowadays is based on silicon. Large progress in this field was under way during past decades. The progress was possible due to reduction of lithographically created circuits like gates and transistors. The technology using properties of doped bulk silicon is reaching its limits. These P-N junctions, that are the cores of any logical circuits, are working only if in its P (or N) part there, have enough dopants, to change the Fermi level of silicon. If the reduction continues, then there will be moment, when there will be no dopants in the silicon, so there will be no P-N junctions and the circuits will not work. Because of this, new approaches of making new more powerful and more energy efficient electronic devices have to be found.

One of the promising ways for making such devices seems to be molecular electronics. Basic idea of the molecular electronic is to use fictionalized organic molecules as small and simple circuits. This approach might lead to small integrated circuits with operating currents of several electrons, instead of mili ampere currents, that are used today. Before the production of circuits from molecules can be started, the electronic properties of adsorbed molecules have to be fully understood. The adsorption will be necessary in order to make stable molecular junctions

The fundamental research on the field of adsorbed molecules on silicon substrates could show us interesting electronic or opto-electronic properties of studied systems. This knowledge can be applied not even for designing of molecular circuits, but also for opto-electronic devices like screens, lasers and diodes. The usage of silicon is supported by the idea that the technology for production molecular circuits on silicon would not differ so much from the technologies nowadays. Thus usage of silicon substrates could lead to the cheaper way to molecular electronics, than other substrates. The one of the most important properties of molecules used for the circuits will be small gap of the molecules. Such molecules are for example aromatic molecules with π-conjugated systems.

The aim of this work is to calculate the electronic properties of several reconstructions of Si (111) surface that have been experimentally observed. Namely it were reconstructions 2×1 *Pandey chain*, 7×7 and several reconstructions with periodicity $\sqrt{3} \times \sqrt{3}\ R30°$. Some of these $\sqrt{3} \times \sqrt{3}$ reconstructions were not proposed in the literature yet. All these reconstructions could be used as substrates for molecular adsorption. Other calculations concern adsorbed benzene molecule on the 7×7 reconstruction of Si (111) surface. Benzene is the smallest aromatic molecule, so its adsorption could work as prototype for more complicated aromatic molecules. The starting points for my calculations were experimental results of Dr. Pavel Kocán, who studied $\sqrt{3} \times \sqrt{3}\ R30°$ reconstruction, and Prof. Alastair McLean, who investigated adsorption of benzene on 7×7 reconstruction. The experimental observations were done mainly by scanning tunnelling microscopy (STM), which enables us to measure the local density of states of surfaces with atomic resolution. The Fireball code, which is based on density functional theory (DFT), was used for the *ab-initio* calculations of the atomic and electronic structures of the studied models. Then the STM simulations of the studied models were done by means of STM code. If the agreement between simulation and

experiment is achieved, then there is very high probability, that the calculated model of atomic structure is the real atomic structure of the surface.

The work is organized as follows: The first chapter contains an introduction to DFT and the fundamentals of the Fireball code. The second chapter concerns bulk terminated Si (111) surface, 2×1 *Pandey chain*, the 7×7 and $\sqrt{3} \times \sqrt{3}$ $R30^\circ$ reconstructions that can be found in the literature. The third chapter consists of theoretical introduction to STM and theory used in the STM code. It also contains a brief description of the experimental arrangement of STM and its operational mode. The first part of fourth chapter consists of procedures and results of experiments made by Dr. Pavel Kocán and Prof. Alastair McLean. The second part concerns results of my calculations, comparison with the experiments and literature and discussion.

1. Density Functional Theory

1.1 *Ab-initio* methods

1.1.1 The stationary Schrödinger equation

All equations are shown in atomic units, unless otherwise specified.

To find any solution to most of statical quantum mechanical systems means finding a solution of the non-relativistic stationary Schrödinger equation [1]:

$$\widehat{H}\,|\Psi_k\rangle = E_k\,|\Psi_k\rangle\,; \tag{1.1}$$

to be more precise, it means to find eigenvectors $|\Psi_k\rangle$ - wave function of the k-th state of the system - and its eigenvalues E_k - k-th energy of the k-th state of the system. The state with minimum energy - E_0 - is called ground state - $|\Psi_0\rangle$ [1].

In this particular work I will focus on systems composed of atoms and electrons, where the wave functions Ψ_k will be many-body wave functions. These wave functions depend on positions of all the nuclei - $\vec{X_A}$ - and all the electrons - $\vec{x_i}$ - of the system. This can be expressed as [1]:

$$|\Psi_i\rangle = |\Psi_i(\vec{X_1},\ldots,\vec{X_A},\ldots,\vec{X_N},\vec{x_1},\ldots,\vec{x_i},\ldots,\vec{x_n})\rangle. \tag{1.2}$$

The operator $\widehat{H}$ in the Schrödinger eq. (1.1) is the Hamiltonian that represents the total energy of the system and therefore it can be written as [1]:

$$H = -\frac{1}{2}\sum_{i=1}^{n}\bigtriangledown_i^2 - \frac{1}{2}\sum_{A=1}^{N}\frac{1}{M_A}\bigtriangledown_A^2 - \sum_{i=1}^{n}\sum_{A=1}^{N}\frac{Z_A}{r_{iA}} + \\ + \sum_{i=1}^{n}\sum_{j>i}^{N}\frac{1}{r_{ij}} + \sum_{A=1}^{N}\sum_{B>A}^{N}\frac{Z_A Z_B}{R_{AB}}. \tag{1.3}$$

The first and second terms of eq. (1.3) are the kinetic energy of the electrons and the nuclei respectively. If we work in cartesian coordinates, the Laplacian operator $\bigtriangledown_q^2$ is defined as [1]:

$$\bigtriangledown^2 = \frac{\partial^2}{\partial x^2} + \frac{\partial^2}{\partial y^2} + \frac{\partial^2}{\partial z^2} \tag{1.4}$$

The other three terms of eq. (1.3) are the potential energy terms. The first of these represents the attractive electrostatic interaction between the nuclei and the electrons, while the other two represent the repulsive interactions between electrons and nuclei respectively. Z_A in eq. (1.3) is the charge of the A-th nuclei. Both r_{pq} and R_{pq} represent the distances between the particles p and q [1, 2].

1.1.2 The Born-Oppenheimer approximation

Solving the Schrödinger eq. (1.1) analytically is impossible for any many-body problem. The only way to finding the solution is to solve it numerically, but some approximations have to be adopted. The most important of these is the

Born-Oppenheimer approximation, which is based on the fact that the mass of the nuclei is about three or even four orders of magnitude higher than the mass of electrons. Thus the electrons move so much faster than nuclei. Consequently, the response of the electrons to modification of the positions of nuclei seems to be immediate in comparison to the speed of nuclei. Therefore, the separation of the motion of the nuclei and the electron is possible and wave function of the whole system can also be divided into two parts. One of which is the wave function of the nuclei - $\Psi_{nuc}(\vec{R_1} \dots \vec{R_N})$ - and second one is wave function of electrons, where the positions of nuclei are just a parameters - $\Psi_{el\ (\vec{X_1} \dots \vec{X_N})}(\vec{r_1} \dots \vec{r_n})$ [1, 2].

Now, the total energy is composed of the energy of the nuclei E_{nuc} and the electrons E_{el} [1]:

$$E_{tot} = E_{nuc} + E_{el} \tag{1.5}$$

and the energy of nuclei can be written [1]:

$$E_{nuc} = \sum_{A=1}^{N} \sum_{B>A}^{N} -\frac{Z_A Z_B}{R_{AB}} + T_{nuc} \tag{1.6}$$

where T_{nuc} stands for the kinetic energy of the nuclei [1].

The energy of the electrons can be obtained by solving electron Schrödinger eq. [1]:

$$\widehat{H}_{el}|\Psi_{el}\rangle = E_{el}|\Psi_{el}\rangle \tag{1.7}$$

where $\widehat{H}_{el}$ is given by [1, 2]:

$$\widehat{H}_{el} = -\frac{1}{2}\sum_{i=1}^{n} \nabla_i^2 - \sum_{i=1}^{n}\sum_{A=1}^{N} \frac{Z_A}{r_{iA}} + \sum_{i=1}^{n}\sum_{j>i}^{N} \frac{1}{r_{ij}} = \widehat{T}_{el} + \widehat{V}_{ext} + \widehat{V}_{ee}. \tag{1.8}$$

1.1.3 The one electron approximation

Even now the reduced Schrödinger eq. (1.7) cannot be solved precisely, because of the electron-electron interaction $\widehat{V}_{ee}$. The first step to finding any solution of eq. (1.7) is to assume, that the many-electron wave function Ψ_{el} can be composed of wave functions of single electrons φ_i. The second step is to replace electron-electron interaction V_{ee} in the electronic Hamiltonian $\widehat{H}_{el}$ by an effective potential V_{ee}^{eff}, that takes into account the interaction of all electrons, but it affects only one electron [1].

In 1928, Douglas Hartree showed that the one-electron approximation results into non-linear system of equations for single electrons wave functions φ_i (see [1] or [2] for more details). Thus Hartree introduced method the called the *self-consistent field* (SCF). At the beginning of any SCF cycle there is provided some guessed set of one electron wave functions φ_i from which the first effective potential V_{ee}^{eff} is obtained. In the second step, the SCF procedure starts to minimize the total energy by the changing one electron functions φ_i, but this modification leads to a new effective potential. The next step is analogy of second one, with new V_{ee}^{eff} potential. This iterative procedure repeats itself until the change of the electron functions and the effective potentials become insignificant. The output of the SCF cycle is an 'exact' set of one electron functions φ_i, where the precision depends on the approximations used and the convergence criteria of the SCF procedure [1].

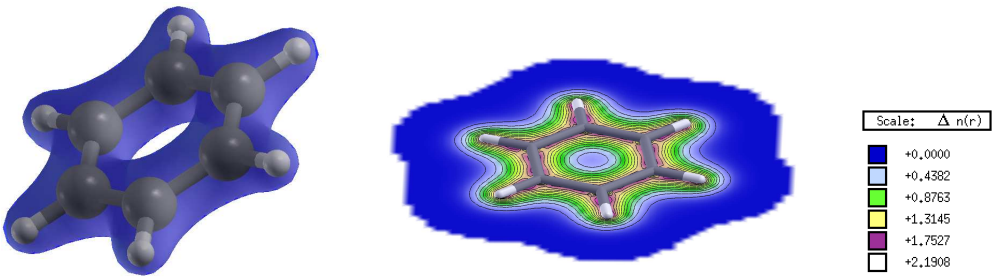

(a) (b)

Figure 1.1: *Representation of the electron density of the benzene molecule*: (a) *three dimensional molecular shape represented by the envelope of constant electronic density (0.7 Au)*, (b) *map showing the values* $\rho(\vec{x})$ *projected onto plane.*

1.2 DFT

1.2.1 Electronic density

1.2.1.1 Basic properties

So far, there are a couple of methods using the one electron approximation. In the field of olid state physics and surface physics, approaches based on the *Density-Functional Theory* (DFT), are the most popular. These methods employ electron density instead of many-body wave functions. Electron density $\rho(\vec{x})$ is an observable quantity, that is an abbreviation for probability density of occurrence of electrons in the volume element $d\vec{r}$ and it can be expressed as [3]:

$$\rho(\vec{r}) = N \int \dots \int |\Psi(r, \vec{r}_2 \dots \vec{r_N})|^2 ds_1 d\vec{r_2} \dots d\vec{r_N}, \tag{1.9}$$

where N is the number of electrons and s is spin. The integration in eq. (1.9) goes over all spins and all the coordinates except coordinates of one electron [3]. Example illustration of electron density of benzene molecule is shown in figure 1.1

The main advantage of using electron density $\rho(\vec{r})$, instead of electron wave function, is a reduction of the many-body problem of N electrons with 3N partial coordinates to 3 spatial coordinates (x, y, z). From the definition (1.9) is clear that the electronic density has positive value and it vanishes at infinity [1]:

$$\rho(\vec{x} \to \infty) = 0. \tag{1.10}$$

By integration of electronic density over whole space we obtain the total number of electrons [1]:

$$N = \int \rho(\vec{r}) d\vec{r}. \tag{1.11}$$

The first attempts of using electronic density for obtaining some part of the electronic energy were made by Thomas and Fermi in 1927. They wrote an prescript for obtaining the coulombic part of the electron-electron interaction and the nuclear-electron interaction. They also approximated kinetic energy of the electrons from model of the uniform electron gas (see [3] for more details).

Later an expression for the exchange energy between electrons was introduced by Thomas, Fermi and Dirac, but this model did not really work. The real DFT was born in 1964, when Hohenberg with Kohn published their two theorems. These theorems postulate that using electron density for ground state calculation instead of many-body wave function is possible [1, 3].

1.2.1.2 The first Hohenberg-Kohn theorem

The first of the Hohenberg-Kohn Theorems proves that any ground state of any many-body system can be uniquely described by an electron density [1].

The proof of the first theorem considers two different electronic Hamiltonian $\widehat{H}_{el} = \widehat{T}_{el} + \widehat{V}_{ee} + \widehat{V}_{ext}$ and $\widehat{H}'_{el} = \widehat{T}_{el} + \widehat{V}_{ee} + \widehat{V}'_{ext}$ that give us two different ground states Ψ and Ψ' respectively, with different corresponding energies E_0 and E'_0. But these ground states have the same electronic density [2].

According to the variational principle, that can be found elsewhere [1, 2, 4], we know that:

$$\left\langle \Psi_0 \left| \widehat{H} \right| \Psi_0 \right\rangle \leq \left\langle \Psi \left| \widehat{H} \right| \Psi \right\rangle \tag{1.12}$$

where $\widehat{H}$ is any Hamiltonian, Ψ_0 is its ground state and Ψ is any state state of the system [1].

The application of the variational principle on our Hamiltonians and states results into [2]:

$$E_0 < \left\langle \Psi'_0 \left| \widehat{H}_{el} \right| \Psi'_0 \right\rangle = \left\langle \Psi'_0 \left| \widehat{H}'_{el} \right| \Psi'_0 \right\rangle + \left\langle \Psi'_0 \left| \widehat{H}_{el} - \widehat{H}'_{el} \right| \Psi'_0 \right\rangle \tag{1.13}$$

We know that these two Hamiltonians differ only in external potential [1]:

$$E_0 < E'_0 + \left\langle \Psi'_0 \left| \widehat{T}_{el} + \widehat{V}_{ee} + \widehat{V}_{ext} - \widehat{T}_{el} - \widehat{V}_{ee} - \widehat{V}'_{ext} \right| \Psi'_0 \right\rangle \tag{1.14}$$

that can be also written [1]:

$$E_0 < E'_0 + \int \rho(\vec{r}) \left[\widehat{V}_{ext} - \widehat{V}'_{ext} \right] d\vec{r}. \tag{1.15}$$

Using the same approach, but with substituted primed and unprimed quantities we obtain [1]:

$$E'_0 < E_0 + \int \rho(\vec{r}) \left[\widehat{V}'_{ext} - \widehat{V}_{ext} \right] d\vec{r}. \tag{1.16}$$

Adding eq. (1.15) and (1.16) gives us a clear contradiction [1]:

$$E_0 + E'_0 < E'_0 + E_0 \tag{1.17}$$

So the conclusion of the first Hohenbergh-Kohn theorem is: an unique ground state electronic density gives an unique external potential. Therefore, the electronic density is a quantity, that enables us to get all the informations about studied system [1].

1.2.1.3 The second Hohenbergh-Kohn theorem

The second Hohenbergh-Kohn theorem defines an energy functional $E[\rho]$ and it proves, that the ground state density ρ_0 minimizes this energy functional [1].

From the first theorem we already know, that any electronic density $\widetilde{\rho}$ defines its own Hamiltonian $\widehat{\widetilde{H}}$ and the external potential $\widehat{\widetilde{V}}_{ext}$ as well as its wave function $\widetilde{\Psi}$. Now, we can simply deduce :

$$\left\langle \widetilde{\Psi} \left| \widehat{H} \right| \widetilde{\Psi} \right\rangle = \widehat{T}[\widetilde{\rho}] + \widehat{V}_{ee}[\widetilde{\rho}] + \int \widetilde{\rho}(\vec{r}) \widehat{V}_{ext} d\vec{r} = E[\widetilde{\rho}] \geq E_0[\rho_0] = \left\langle \Psi_0 \left| \widehat{H} \right| \Psi_0 \right\rangle . \quad (1.18)$$

Written in a simpler way:

$$E_0 \leq E[\widetilde{\rho}] = \widehat{T}[\widetilde{\rho}] + \widehat{V}_{ee}[\widetilde{\rho}] + \int \widetilde{\rho}(\vec{r}) \widehat{V}_{ext} d\vec{r}, \quad (1.19)$$

which is nothing else than the variational principle for the electronic density ρ [1].

1.2.2 The Kohn-Sham equation

Later Kohn and Sham found a simple functional $E[\rho(\vec{r})]$ which is based on the theory of non-interacting electron gas - the so called Jellium model. Unlike the first attempts made by Thomas, Fermi and others which was based strictly on electron density, Kohn and Sham postulated that the wave function of the whole system Ψ_{KS} is a Slater determinant composed of pseudo-one electron spin orbitals φ_i^{KS}. This set of pseudo-spin orbitals is orthonormal, so the electronic density can be written [1]:

$$\rho(\vec{r}) = \sum_{i=1}^{n} |\varphi_i^{KS}(\vec{r})|^2. \quad (1.20)$$

To obtain ground state density $\rho_0(\vec{r})$ we need to self-consistently iterate the Kohn-Sham orbitals $\varphi_i^{KS}(\vec{r})$ (similarly as in Hartree-Fock procedure - see [1] or [3]).

It can be shown (see [1] for example) that a single determinant wave function Ψ_{KS} is an exact wave function for system of non-interacting fermions (e.g. non-interacting electron gas). In this case, the exact kinetic energy T_s can be obtained [1]:

$$T_s = -\frac{1}{2} \sum_{i=1}^{n} \left\langle \varphi_i^{KS}(\vec{r_i}) \left| \nabla^2 \right| \varphi_i^{KS}(\vec{r_i}) \right\rangle . \quad (1.21)$$

But in case of interacting electrons, this kinetic energy is not the right one. Therefore for total energy calculations some correction of the kinetic energy has to be adopted (it will be shown later) [1].

Knowing this, the energy of the whole system can be expressed as [1]:

$$E[\rho(\vec{r})] = T_s[\rho] + J[\rho] + E_{XC}[\rho] + E_{Ne}[\rho] =$$

$$= -\frac{1}{2} \sum_{i=1}^{n} \int \varphi_i^{KS}(\vec{r_i}) \bigtriangledown^2 \varphi_i^{KS}(\vec{r_i}) d\vec{r_i} + \frac{1}{2} \int \int \frac{\rho(\vec{r_1})\rho(\vec{r_2})}{r_{12}} d\vec{r_1} d\vec{r_2} + E_{XC}[\rho(\vec{r_1})] +$$

$$+ \int \rho(\vec{r_1}) V_{Ne}(\vec{r_1}) d\vec{r_1}, \quad (1.22)$$

where the second term - $J[\rho]$ - is the coulombic repulsion between electrons and last term - $E_{Ne}[\rho]$ -is the interaction between the electrons and the nuclei. The $E_{XC}[\rho]$ is the so called *exchange-correlation energy* or *exchange-correlation functional* (XC - functional) and it contains the residual part of the true kinetic energy - T_C - and the quantum electron-electron interaction E_{Qee} [1]:

$$E_{XC}[\rho] = (T[\rho] - T_s[\rho]) + (E_{ee}[\rho] - J[\rho]) = T_C[\rho] + E_{Qee}[\rho]. \tag{1.23}$$

By applying the variational principle to eq. (1.22) we can find the condition for minimizing the whole energy, together with maintaining the orthonormality of the one electron wave functions. This condition results into set of equations for all one electron functions φ_i^{KS} (see [3] for detailed derivation) [1]:

$$\left(-\frac{1}{2}\bigtriangledown^2 + \left[\int \frac{\rho(\vec{r_2})}{r_{12}} d\vec{r_2} + V_{XC}(\vec{r_1}) - \sum_{A=1}^{N} \frac{Z_A}{r_{1A}}\right]\right)\varphi_i^{KS} = \varepsilon_i \varphi_i^{KS}. \tag{1.24}$$

Where the *exchange-correlation* potential V_{XC} is defined [1]:

$$V_{XC} = \frac{\partial E_{XC}[\rho]}{\partial \rho}. \tag{1.25}$$

Up to this point, there are no other approximations than the ones made by Born-Oppenheimer and one-electron approximation. The main problem is, neither E_{XC} nor V_{XC} are known. Therefore they must be somehow approximated [1].

1.2.3 The exchange-correlation functionals

1.2.3.1 LDA

Nowadays there are a couple of approaches for obtaining the *exchange-correlation energy*; the first and the most simple is called the *Local-Density Approximation* (LDA). That means, that *exchange-correlation energy* E_{XC} depends only on the local amount of the electric density $\rho(\vec{r})$ [1]:

$$E_{XC}^{LDA} = \int \rho(\vec{r}) \varepsilon_{XC}[\rho(\vec{r})] d\vec{r}, \tag{1.26}$$

where ε_{XC} is a normalized *exchange-correlation energy* per one particle of the uniform electron gas on which the whole idea of LDA is based. The normalized energy ε_{XC} can be divided into pure exchange $\varepsilon_X[\rho(\vec{r})]$ and correlation $\varepsilon_C[\rho(\vec{r})]$ contributions [1]:

$$\varepsilon_{XC}[\rho(\vec{r})] = \varepsilon_X[\rho(\vec{r})] + \varepsilon_C[\rho(\vec{r})]. \tag{1.27}$$

The equation, for obtaining exchange energy $\varepsilon_X[\rho(\vec{r})]$ from uniform electron gas was derived by Bloch and Dirac in late 1920's [1]:

$$\varepsilon_X[\rho(\vec{r})] = -\frac{3}{4}\sqrt[3]{\frac{3\rho(\vec{r})}{\pi}}. \tag{1.28}$$

On the other hand, no simple expression for correlation energy $\varepsilon_C[\rho(\vec{r})]$ exists. The most common way to get it is through quantum Monte-Carlo simulations. The first were made by Ceperly and Alder in 1980 (see [5] for more details).

LDA gives satisfying results for systems that are close to the model of the uniform electron gas, such as metals. On the contrary, the results are not so good for molecules, because LDA has a tendency to overestimate the strength of chemical bonds and it also usually produces small gaps for any system [1, 6].

1.2.3.2 GGA

The fact that LDA does not work so well for molecules is caused by the electron density variations which are much larger, than in metals or solid states in general. The problems, which LDA has with molecules, show us, that other information than just electronic density is necessary. Thus, method called the *generalized-gradient approximation* (GGA) was invented. This functional takes into account not only electronic density, but also its gradient:

$$E_{XC}^{GGA} = \int \rho(\vec{r}) F[\rho(\vec{r}), \bigtriangledown\rho(\vec{r})] d\vec{r}, \tag{1.29}$$

where $F[\rho(\vec{r}), \bigtriangledown\rho(\vec{r})]$ is some general functional. So far, there is a number of different GGA functionals - B88 [7], PW91 [8], PBE [9], LYP [10] and so on. (See e.g. [1] for more details and comparison) These functionals give us better results than LDA functionals for some systems, mainly for molecules. But generally speaking, they still are not enough accurate for counting of binding energy with smaller error than 1 kcal/mol (so called chemical accuracy) [11].

1.2.4 Numerical Implementations

1.2.4.1 Introduction

In next two chapters we will describe the main numerical aspects for solving Kohn-Scham equations.

1.2.4.2 Pseudopotentials

The core electrons of atoms are involved merely in chemical reactions. They are practically intact when atoms form a solid state. So we can dispose of the core states by means of pseudopotentials in the calculations. The main advantage of pseudopotentials is in speeding up calculations, due to reducing the electronic problem only to valence electrons. Thus the original Schrödinger eq. for valence electrons [11]:

$$H\psi_i^v(\vec{r}) = \left(-\frac{1}{2}\sum_{i=1}^{n} \bigtriangledown^2 + V(\vec{r})\right) \psi_i^v(\vec{r}) = \varepsilon_i^v \psi_n^v(\vec{r}), \tag{1.30}$$

where $V(\vec{r})$ is the total effective potential, can be changed into [11]:

$$H\widetilde{\psi}_i^v(\vec{r}) = \left(-\frac{1}{2}\sum_{i=1}^{i} \bigtriangledown^2 + V_{PS}(\vec{r})\right) \widetilde{\psi}_i^v(\vec{r}) = \varepsilon_n^v \widetilde{\psi}_i^v(\vec{r}), \tag{1.31}$$

where $\widetilde{\psi}_i^v$ is pseudo-valence eigenfunction and $V_{PS}(\vec{r})$ is pseudopotential, that can be obtained from *ab-inito* calculations, or an *empirical* pseudopotentials can be

used. The*empirical* pseudopotentials are fitted to reproduce experimental data [11].

The pseudopotentials can also include the relativistic effects that are appreciable for large atoms as tungsten. Another advantage of pseudopotentials is that they enable us to decrease the number of basis set functions so then calculations of larger systems are possible. On the other hand, pseudopotentials can make the calculations less accurate, due to 'freezing' of core eigenenergies ε_n^c and core wave functions φ_n^c. Once the pseudopotential is made from them, it becomes fixed and therefore it cannot respond to any changes of the environment. Second disadvantage is that all the information about core states is lost. [12, 11]

1.2.4.3 Basis sets

Numerical solution requires us to express the wave functions in basis set. There are several approaches; each possesses its advantages and drawbacks. In case of usage of one electron approximation, the one electron wave function φ_i is represented by coefficients c_{ki} in its basis μ_k [11, 12]:

$$\varphi_i = \sum_{k=1}^{N} c_{ki}\mu_k. \tag{1.32}$$

The *plane waves* are very popular in the solid state physics (see [12] for more details), but in this work I will focus on the *linear combination of atomic orbitals* (LCAO) method [11].

The concept of the *linear combination of atomic orbitals* was introduced in late 1920's. The one electron wave function φ_i - called *molecular orbital* - is comprised of atomic orbitals $\mu_k = \mu_{\alpha nlm}(\vec{r} - \vec{R}_\alpha)$. The original index k has four parts now: α, n, l and m. α signs that the orbital belongs to α-th atom, that has its centre in $\vec{R}_\alpha$. The other indices n, l and m correspond to principal, azimuthal and magnetic quantum number of orbital respectively. Any orbital function $\mu_{\alpha,n,l,m}$ can be decomposed into its radial $R_{nl}(r)$ and spherical part $Y_{lm}(\theta, \phi)$. If we make an assumption that the α-th atom is in the centre of coordinates - $\vec{R}_\alpha = \vec{0}$, then it can be written [11]:

$$\mu_{\alpha nlm}\left(\vec{r} - \vec{R}_\alpha\right) = \mu_{nlm}(\vec{r}) = R_{nl}(r)Y_{lm}(\theta, \phi), \tag{1.33}$$

where $Y_{lm}(\theta, \phi)$ are the spherical harmonics. Unlike the spherical harmonics, which are clearly defined, several types of the radial functions R_{nl} can be used. Analytical radial functions as *Slate Type Orbitals*, or *Gaussian Type Orbitals* (see [1, 4] for more details), are quite often used. But the radial functions can be obtained numerically from solving Schrödinger equation for single atom, too [11].

1.3 Periodic systems - Bloch's theorem

In any periodic system, the atoms are periodically organized, so the electrostatic potential of the nuclei have to fulfil the condition [13]:

$$U(\vec{r}) = U(\vec{r} + \vec{T}), \tag{1.34}$$

where $\vec{T}$ is any translation vector of the periodic (Bravais) lattice. Schrödinger equation for a single electron in the periodic potential can be written [13]:

$$H\psi_n = \left(-\frac{1}{2}\sum_{i=1}^{n} \bigtriangledown^2 + U(\vec{r})\right)\psi_n = \varepsilon_n \psi_n. \tag{1.35}$$

Bloch theorem tells us that the solution of eq. (1.35) for the electron's eigenstates is the Bloch wave [13]:

$$\psi_{n\vec{k}}(\vec{r}) = e^{i\vec{k}\vec{r}} u_{n\vec{k}}(\vec{r}), \tag{1.36}$$

where n is principal quantum number and $\vec{k}$ is so called wave vector. The wave function $u_{n\vec{k}}(\vec{r})$ is also periodic [13]:

$$u_{n\vec{k}}(\vec{r}+\vec{T}) = u_{n\vec{k}}(\vec{r}). \tag{1.37}$$

When the Bloch wave is substituted into Schrödinger eq. (1.35) it can be easily derived that the eigenenergies ε_n depend on the wave vector $\vec{k}$. Therefore wave vector $\vec{k}$ is a quantum number. The energy $\varepsilon_{n,\vec{k}}$ for fixed n is called electron band and set of these energies for periodic system is called a band structure [13]. The example of the band structure for Si bulk can be found on figure 1.2.

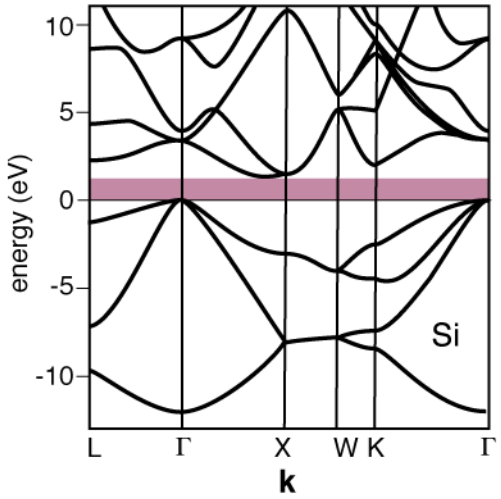

Figure 1.2: *The band structure of Silicon. On the x axis are different* $\vec{k}$ *of the first brillouin zone.* Figure taken from P. Hofmann [14]

1.4 The Fireball code

The Fireball code [15] is an *ab-initio* computational package based on DFT, which can calculate atomic and electronic structure of clusters and periodic systems. It uses the formalism of norm-conserving pseudopotentials [16] and LCAO with the localized pseudo-atomic orbitals basis sets. This pseudo-atomic orbitals called *Fireball* orbitals have the same form as it was introduced in eq. (1.33) but these

numerical orbitals have numerical radial functions $R_{nl}^{Fireball}(r)$ with a radial cut in some distance from nuclei r_c, that means [17]:

$$R_{nl}^{fireball}(r \geq r_c) \equiv 0. \tag{1.38}$$

Due to radial cut the *Fireball* orbitals are slightly excited in comparison with the real atomic orbitals, that become zero for $r \to \infty$. Example of the *Fireball* radial functions for oxygen can be found on figure 1.3. The main advantage of the *fireball* orbitals are that an overlap of two orbitals is zero, when the centres of the orbitals are in distance bigger than sum of their radial cuts. Then their interaction becomes zero, too [17].

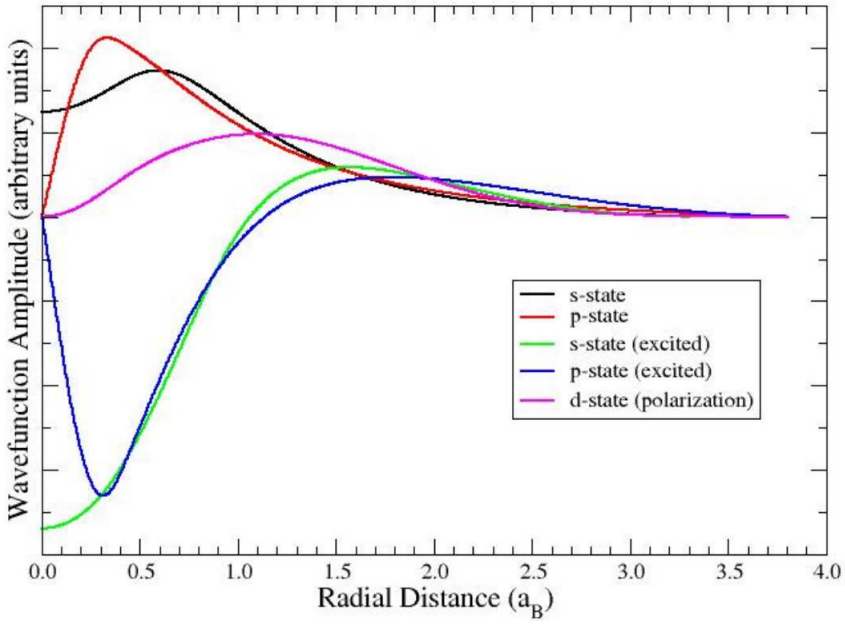

Figure 1.3: *The local pseudo-atomic orbitals for oxygen. The basis shown is double numerical in s and p, with a d polarization state.* Figure taken from J. Lewise et al. [17]

The core of the Fireball code is an approximate self-consistent extension of Harris-Foulkes functional [17]:

$$E_{tot}^{Harris} = E^{BS} + \Big(U^{ion-ion} - U^{ee}[\rho_{in}(\vec{r})]\Big) + \Big(U^{XC}[\rho_{in}(\vec{r})] - v^{XC}[\rho_{in}(\vec{r})]\Big). \tag{1.39}$$

The main difference between the Harris-Foulkes functional and the Kohn-Sham functional is that the first is defined entirely in the terms of an input electron density - $\rho_{in}(\vec{r})$, while second one is defined in terms of both, input and output density. The term E^{BS} in eq. (1.39) is an energy of band structure [17]:

$$E^{BS} = 2\sum_i \varepsilon_i, \tag{1.40}$$

where i runs through all occupied energy levels ε_i, which were gained as eigenvalues from one-electron Schrödinger equation [17]:

$$\Big(-\frac{1}{2}\bigtriangledown^2 + V_{ext}(\vec{r}) + \mu^{XC}[\rho_{in}(\vec{r})] + \frac{1}{2}\int \frac{\rho_{in}(\vec{r})}{|\vec{r}-\vec{r'}|} d^3\vec{r'}\Big)\psi_i(\vec{r}) = \varepsilon_i\psi_i(\vec{r}), \tag{1.41}$$

where μ^{XC} is the exchange-correlation potential of one electron, that can be obtained from the exchange-correlation energy of one electron ε^{XC} [1]:

$$\mu^{XC} = \frac{\partial \varepsilon^{XC}[\rho_{in}(\vec{r})]}{\partial \rho_{in}(\vec{r})}. \tag{1.42}$$

$U^{ion-ion}$ in eq. (1.39) is the coulombic interaction between nuclei [17]:

$$U^{ion-ion} = \frac{1}{2} \sum_{i,j} \frac{Z_i Z_j}{|\vec{R}_i - \vec{R}_j|}, \tag{1.43}$$

whereas U^{ee} is the coulombic interaction between electrons [17]:

$$U^{ee} = \frac{1}{2} \int \frac{\rho_{in}(\vec{r})\rho_{in}(\vec{r'})}{|\vec{r} - \vec{r'}|} d^3\vec{r} d^3\vec{r'}, \tag{1.44}$$

The last two terms of eq. (1.39) are the exchange-correlation's correction, given by [17]:

$$\Big(U^{XC}\rho_{in}(\vec{r})] - v^{XC}[\rho_{in}(\vec{r})]\Big) = \int \rho_{in}(\vec{r})\Big(\varepsilon^{XC}[\rho_{in}(\vec{r})] - \mu^{XC}[\rho_{in}]\Big) d^3\vec{r}. \tag{1.45}$$

The correction is necessary, because eigenenergies gained from the one-electron Schrödinger equation (1.41) depend on the exchange-correlation potential μ^{XC}, but the correct exchange-correlation energy is obtained from ε^{xc} [17].

The exchange-correlation energy is evaluated in Fireball by the McWEDA method, which was proposed by Jelínek et al. [18]. This method enables us to calculate exchange-correlation energies of up to three interacting atoms and store them in a table. These pre-calculations and advantages of *fireball* orbitals speed up calculations and make calculations of large system composed of thousand of atoms possible. The McWEDA method can be adopted for any type of the XC-functional; but in this work I will use LDA with the Perdew-Zunger parameterisation [19] of the correlation energy of a homogeneous electron gas calculated by Ceperley-Alder [20].

To obtain the real ground state of any calculated structure the geometry optimization is needed. To find an optimal geometrical structure, Fireball moves the atoms in the direction of forces, obtained by [21]:

$$\vec{F_\alpha} = \frac{\partial E_{tot}}{\partial \vec{R_\alpha}}, \tag{1.46}$$

where $\vec{F_\alpha}$ is the force that affects atom α sitting in position $\vec{R_\alpha}$. For the derivation Hellman-Feynman theorem is used (see [21] for more details). This approach enables us to pre-calculate the forces and store them, too [17].

More information about the Fireball can be found on the Fireball web site [15].

2. Si (111) surface

2.1 Introduction to surfaces

While in ideal mono-crystal are 3D periodic conditions and every atom has its constant number of nearest neighbours (four in the case of silicon), on the surface one dimension of periodicity is lost, because of cutting of crystal in a plane. Also at least one layer of atoms is disrupted by the fact that its atoms lost minimally one neighbour. These circumstances induce new electronic states different from bulk states and they cause energetic unfavourableness of bulk terminated surfaces. That leads to relaxations - usually connected with changes of inter-layer distances of the surface and few under-surface layers - and reconstructions when the atoms reorganize themselves so much that the original periodicity of the surface is lost. Some reconstructions can affect only few topmost atoms, whereas other like 7×7 DAS (see chapter 2.3.3) are more complex and affect more than four layers [22, 23].

In the case of semiconductors, especially silicon, the atoms are strongly bond in the bulk by covalent bonds. When one of the atoms loses one of its nearest neighbours, then the covalent bond is broken and the so called dangling bond appears, with one non-pair electron in it. The dangling bonds are very local and they bind the Fermi Level on themselves (*Fermi Level pinning*). So, all the non-reconstructed semiconductors' surfaces are extremely reactive due to the presence of at least one dangling bond on the topmost atoms. The dangling bonds cause metallic behaviour of the surface atoms and they are energetically unfavourable. Thus the semiconductors surfaces are almost in all cases reconstructed in order to get rid of the dangling bonds [22, 23].

Under different conditions different reconstructions can appear. Because these reconstructions have different periodicity and also they might be some vacancies or extra atoms, there is no straightforward way how to compare their energetic favourableness. Even, if the surface is composed of one element. In the literature there have been proposed few formulas, but in this work I will use the formula, that was used e.g. by A. A. Stekolnikov et. al. [24]. This formula gives us favourableness $\alpha_{m\times n}$ of a $m \times n$ reconstruction versus a bulk terminated surface - imaginary surface in which are the atoms on the same positions as they are in crystal [24]:

$$\alpha_{m\times n} = \frac{E^{TOT}_{m\times n}}{m \times n} - E^{TOT}_{1\times 1} - \gamma \left(\frac{N_{m\times n}}{m \times n} - N_{1\times 1} \right), \tag{2.1}$$

where $E^{TOT}_{m\times n}$ is the total energy of the $m \times n$ and $E^{TOT}_{1\times 1}$ is the energy of one unit cell of the bulk terminated surface. If there are any vacancies or extra atoms, then $\alpha_{m\times n}$ depends on chemical potential γ of the atom (in this work it is silicon atom). The chemical potential of atoms on the surface has to be bigger than the energy of one atom in the bulk and at the same time smaller than the energy of a single atom in the vacuum. The term $N_{m\times n}$ is the number of atoms in the $m \times n$ reconstruction, while $N_{1\times 1}$ stands for the number of one unit cell of the bulk terminated surface. So if α is lower than zero, that means the reconstruction is more favourable than the bulk terminated surface [24].

2.2 Bulk terminated Si (111) surface

If the atoms of the silicon surface, which was cut in the Müller plane (111), would not change their positions, then it would be ended by a layer, in which every Si atom has only three neighbours and one dangling bond. Such surface is called the bulk terminated Si (111) surface and its atomic structure is shown on the figures 2.1 and 2.2. The dangling bonds are oriented perpendicular to the surface, as you can see on the figure 2.2 [22, 23].

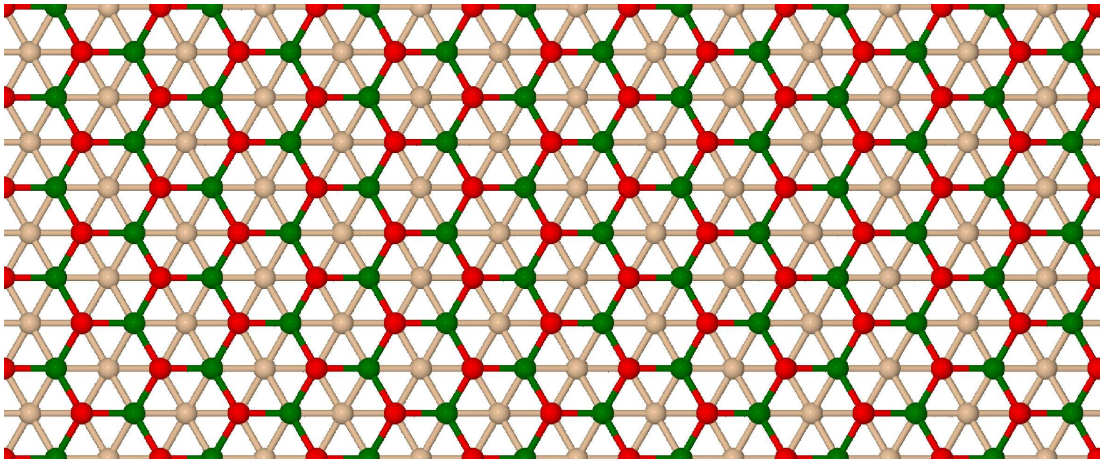

Figure 2.1: *Top view of the bulk terminated Si (111) surface. The topmost atoms are coloured red, the atoms of second layer are coloured green.*

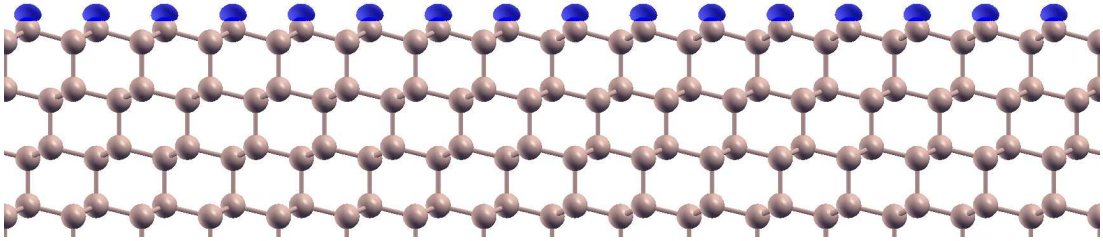

Figure 2.2: *Side view of eight layers of the bulk terminated Si (111) surface with real-space projections of the dangling bonds (blue).*

In the electronic structure of the bulk terminated surface, there are several differences compared to the bulk of Si. Together with the half-filled dangling bonds, which are situated on the Fermi level, also some *back-bond* resonances appear. These resonances try to compensate the loss of bonds across the cleavage plane and they are localized between first few atomic layers of the Si (111) surface. The *back-bonds* also strengthen the attachment of the surface atoms to their subsurface neighbours [22].

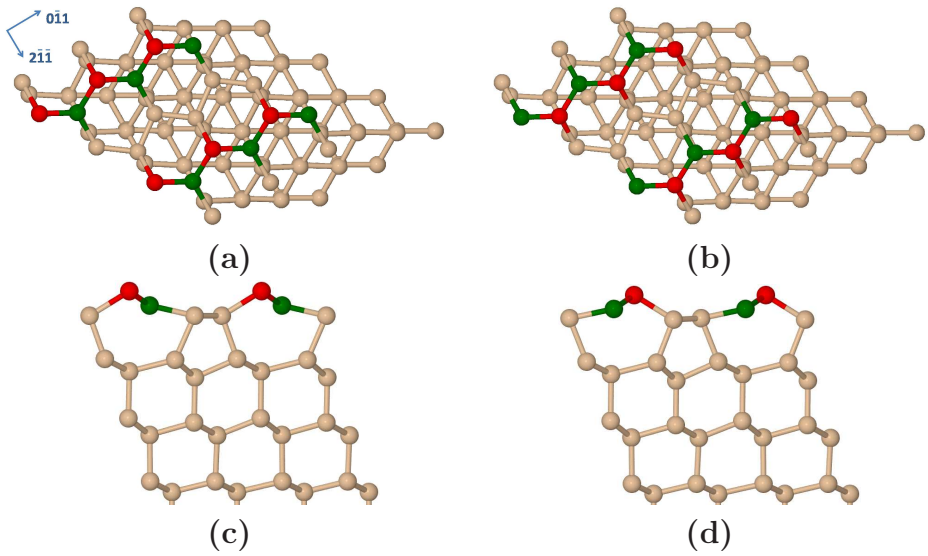

Figure 2.3: *Top view of* **(a)** *the left chain isomer and* **(b)** *righr chain isomer of 2×1 reconstruction. Side view of* **(c)** *the left chain isomer and* **(d)** *the right chain isomer of the 2×1 reconstruction. The up atoms are red; the down atoms are the green ones.*

2.3 Reconstructed surfaces

2.3.1 2×1 *Pandey chain*

As mentioned previoulsy, the dangling bonds make the bulk terminated surface unstable, so the clean silicon (111) surface is always reconstructed, even after cleavage. The one of the most energetically favourable reconstructions, but still only metastable, is the 2×1 *Pandey chain* reconstruction. This reconstruction can be observed on the surface, even after cleavage of the surface at low temperature, due to a very low activation barrier for reconstructing of the surface [23]. The 2×1 *Pandey chain* reconstruction was first proposed by Pandey in 1981. [25]. Especially two surface silicon layers are affected by the reconstruction, as you can see on the figure 2.3. Its topmost atoms are arranged into the chains with double bonds - σ and π - with each other. There are two isomers of this reconstruction. Each isomer has different direction of the buckling of the atoms of the chains. The buckling causes the charge transfer from the down atom (green in the figure 2.3) to the up atom (red) and the splitting of the bonding and the anti-bonding π-bands. Thus this arrangement eliminates the dangling bonds and it also causes that 2×1 *Pandey chain* reconstruction has a gap, that depends on the isomerization. In the literature [26, 24] there can be found, that the left chain reconstruction is slightly energetically favourable, with a gap of about 0.3 eV, while the right chain reconstruction has a gap of about 0.7 eV, that much better corresponds to the experimental observations. DFT-LDA calculations made by Garleff et al. [26] and Stekolnikov et al. [24] show that the energetic difference between left and right chain is about 0.01 eV that is much lower value than the accuracy of DFT-LDA. The difference of the height between up and down atoms was calculated as 0.51 Å for the right chain isomer by Garleff et al. [26]. Stekolnikov et. al. [24]

computed this height difference to be 0.53 Å for the right chain isomer and 0.63 Å for the left chain isomer.

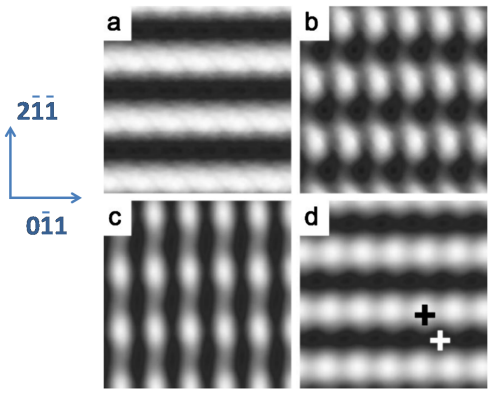

Figure 2.4: *The experimental STM maps of 2×1 Pandey chain reconstruction of Si (111) surface taken with constant current mode for bias voltages and currents:* **a** *- +1.4 V; 0.5 nA.* **b** *- + 0.6 V; 0.5 nA.* **c** *- -0.4V; 0.1 nA* **d** *- -1.1V; 0.2 nA.* Figure taken from Garlef et al. [26]

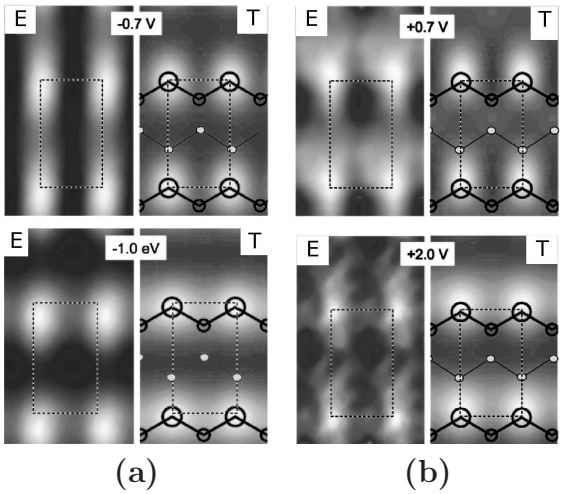

Figure 2.5: *The experimental and simulated STM maps of 2×1 Pandey chain. Left collumn -* **(a)** - shows the maps for negative bias voltages (filled states) - 0.7 V (atop) and - 1.0 V below. Right column **(b)** *shows the maps for positive bias voltages (empty states) + 0.7 V (atop) and + 2.0 V below. The experimental maps are marked as* **E**, *while the simulations are market as* **T**. Figure taken from Garlef et al. [26]

The STM (see chapter 3) experiments and simulations show, that in the negative bias voltages (the filled states of the sample) the up atoms seem always as bright spots in the STM maps, while in the low positive bias voltages (the empty states of the sample) the bright spots corresponds with down atoms. However when the voltage is over 0.7 V the tunnelling to up atoms starts to dominate again - see figures 2.4 and 2.5 [26].

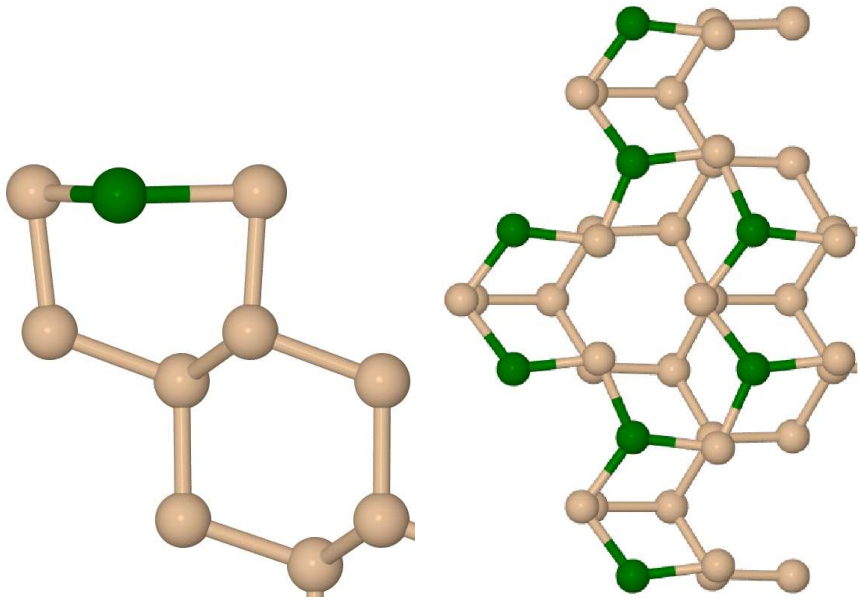

(a) **(b)**

Figure 2.6: *The $\sqrt{3} \times \sqrt{3}$ $R30°$ reconstruction with one vacant atom in the top layer - vacancy reconstruction:* **(a)** *Side view of one unit cell;* **(b)** *Top view of four unit cells. The green topmost atoms arrange themselves into the same height as the atoms of the second layer during reconstruction.*

2.3.2 $\sqrt{3} \times \sqrt{3}$ $R30°$ reconstructions

The $\sqrt{3} \times \sqrt{3}$ $R30°$ is quite common reconstruction of any modified Si (111) surface by metals; e.g. silver [27], lead [28], gallium [29] and so on. Whereas for the clean surface this reconstruction is quite uncommon. In the literature only two experimental observations can be found [30, 31].

The first of them was observed after intensive bombarding of the surface with argon ions and then it was rapidly heated up to 1000°C and maintained there for 5 sec. Then the surface was rapidly cooled to 20°C. The $\sqrt{3} \times \sqrt{3}$ $R30°$ pattern was observed by the low energy electron diffraction (LEED). The atomic structure was proposed by fitting of LEED I-V curves. The observed reconstruction has one vacant top layer atom in the unit cell, as you can see on the figure 2.6 [30]. In this work I will call this reconstruction *vacancy*.

The second observation was made by the STM, after depositing of 0.05 ML of the silicon onto the disordered "1×1" surface. After this procedure, quite large areas of the so called $\sqrt{3} \times \sqrt{3}$ *adatom* reconstruction were found [31]. In this reconstruction there is extra atom added. This extra atom called adatom can sit in two stable positions - T_4 and H_3. In the second case the adatom has just three neighbours below it, as you can see on the figure 2.7 (b), while in the first one there are already mentioned three atoms plus one another atom of the second layer just under the adatom - the figure 2.7 (a). Solares et al. [32] has shown, that the T_4 position is much more energetically favourable, due to much larger delocalization of the highest occupied molecular orbital (HOMO), than in the case of the H_3.

There is also one theoretical work about $\sqrt{3} \times \sqrt{3}$ $R30°$ reconstruction by

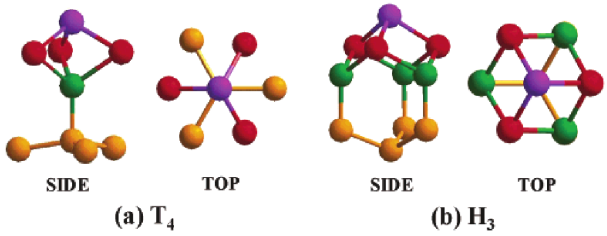

Figure 2.7: *The schematic drawings of models of adatom sitting in T_4 position* **(a)** *and in H_3 position* **(b)**. The figure is taken from D. Solares et al. [32]

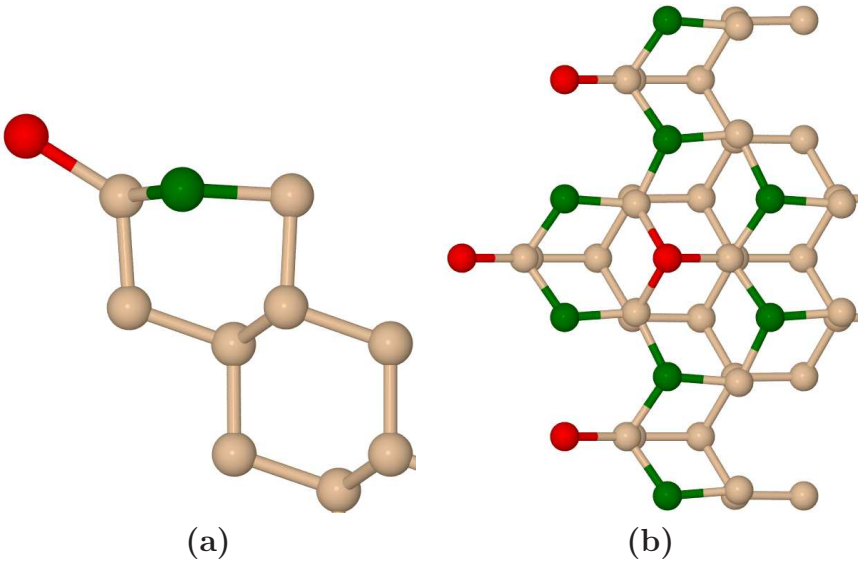

Figure 2.8: *The $\sqrt{3} \times \sqrt{3}$ $R30°$ buckled reconstruction:* **(a)** *Side view of one unit cell;* **(b)** *Top view of four unit cells. Up atoms are red; Down atoms are the green ones.*

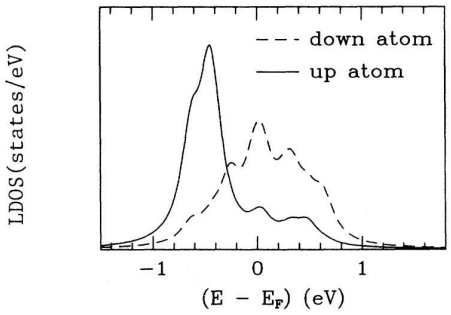

Figure 2.9: *Calculated LDOS of buckled reconstruction for Up atom (full line) and down atom (dashed line)* . Figure taken from F. Ancilotto et al. [33]

F. Ancilotto et. al. [33], that proposed a reconstruction called *buckled*. In this reconstruction is one of three atoms of top layer raised up - upatom - while the other two are moved slightly down - downatom, as you can see on the figure 2.8. F. Ancilotto et. al. computed that the *buckled reconstruction* is more energetically favourable then the vacancy structure, but the 2×1 *Pandey chain* reconstruction is still the most favourable of this three reconstructions. In order to found the stability of the buckled reconstruction F. Ancilotto et al [33] used dynamical simulations. They found out, that the *buckled* reconstruction is not even metastable, because there is no barrier against turning into the 2×1 *Pandey chain*. On the other hand they observed, that one vacancy per many unit cells (four unit cells in this case) makes the *buckled* reconstruction metastable. They also calculated the local density of states (LDOS) for the up and down atoms as you can see on the figure 2.9 [33].

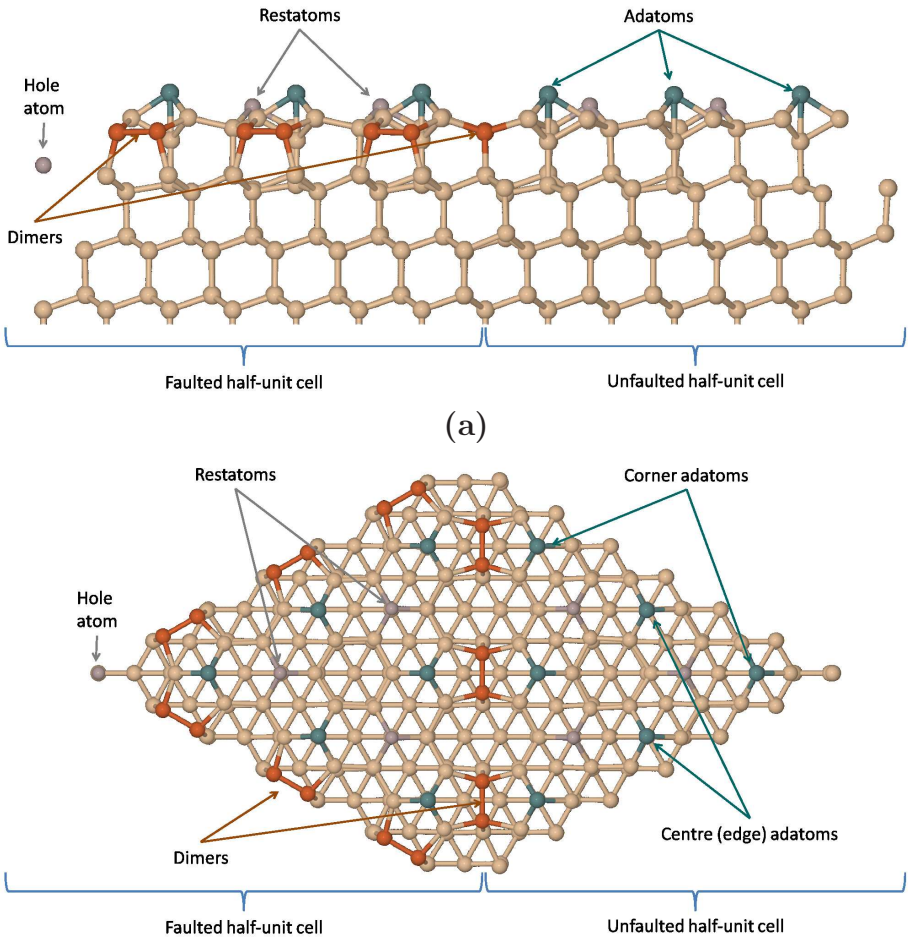

Figure 2.10: *The atomic structure of 7×7 DAS reconstruction*:**(a)** *Top view of 7×7 unit cell;* **(b)** *Side view of 7×7 unit cell.*

2.3.3 7×7 DAS

The 7×7 dimer-adatom-stacking-fault (DAS) reconstruction (or the 7×7 for short) is the most stable reconstruction of the Si (111) surface. The atomic structure is shown in the figure 2.10. Its structure was proposed by Takayanagi et al. in 1985 [34] for the first time. Later this model was corrected many times. The stability of the reconstruction is caused by the very effective treatment of the dangling bonds. The stacking fault, that occurs in the first two layers in one half of the 7×7 unit cell leads to the dimers on the borders of the stacking fault and only 42 dangling bonds in the first layer. In addition 36 of these dangling bonds are fully saturated by added silicon atoms - adatoms. The total number of dangling bonds per the 7×7 unit cell is 19 [23]. Twelve of them are situated on adatoms, six are situated on restatoms and one is on the corner hole atom. The adatoms (the zero layer) sit in the T_4 position, while the restatoms are the highest atoms of the first layer. The corner hole atom is the atom of the third layer surrounded by a twelve-membered ring of atoms of the first and second layer [32]. The faulted and the unfaulted halves of the unit cell are distinguished by mentioned stacking pattern. Some of the energy gained from reduction of the dangling bonds is con-

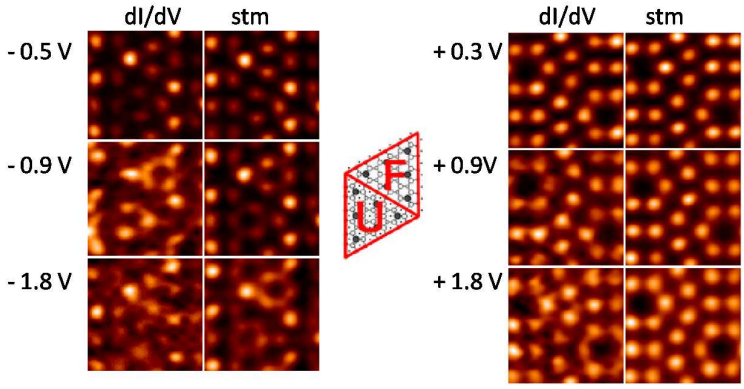

Figure 2.11: *Constant height STM images together with dI/dV maps for different bias voltages.* Figure taken from Švec et al. [37].

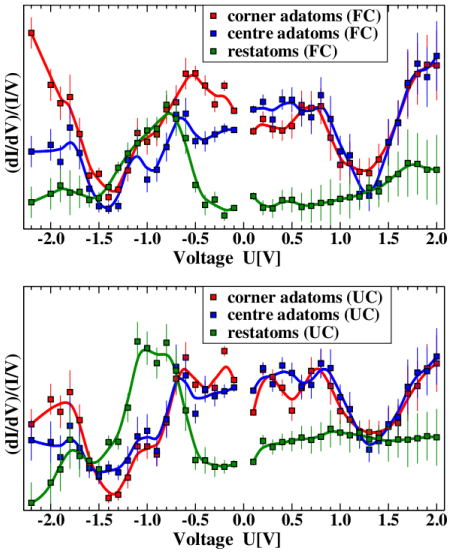

Figure 2.12: *Obtained dI/dV spectra of important surface atoms of 7×7 reconstruction.* Figure taken from Švec et al. [37]

sumed by the stacking fault [22]. Depending in which half-cell are the adatoms and restatoms situated they can be classified as *faulted* and *unfaulted*. For the adatoms other classification can be made, according to where are they situated in the half-unit cell - see figure 2.10. So the adatoms are named faulted corned - *fc*, faulted edge (or centre) - *fe*, unfaulted corner - *uc* - and unfaulted edge (centre) - *ue* [22, 32]. In this work I will label restatom in the faulted half unit cell as *fr* and in the unfaulted half unit cell as *ur*.

To decrease the energy even more, there are significant changes in the electronic structure. The charge transfer from the adatoms to the the restatoms fills the restatom dangling bond. Due to the stacking fault, the halves of the unit cells differ from each other also in the electronic structure and reactivity. The faulted half unit cell is slightly more reactive and its adatoms are brighter in the STM images, when positive bias voltage is applied, as you can see on the figure 2.11. [35, 36, 37].

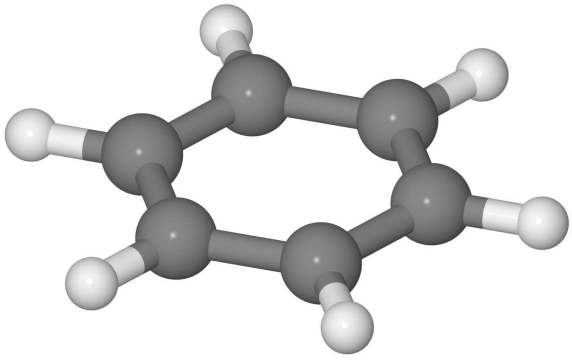

Figure 2.13: *The atomic structure of the benzene molecule.*

2.3.4 The chemisorption of benzene on 7×7 DAS

In this work I also studied reactions of adsorbate with the silicon surface. The chosen adsorbate is the benzene molecule. The studied system was benzene chemisorbed on the most stable reconstruction of Si (111) surface - the 7×7 DAS.

The benzene molecule - C_6H_6 - is a ring with a conjugated system of π bonds (see figure 2.13), that makes the molecule chemically stable. Benzene is the smallest and simplest aromatic molecule with a gap of about 13 eV [38].

The adsorption of benzene on Si(111) has been studied extensively during past two decades by wide variety of surface analysing techniques [39]-[50]. These studies shown, that at low temperature ($\leq$ 120 K) the benzene adsorbs without any changes of its geometry, thus it physisorbs. However, at room temperature, the benzene is strongly bonded with the substrate - it chemisorbs. This was proved by the thermal desorption spectroscopy (TDS). Two different bonding energies were found for the chemisorbed benzene - 0.91 eV and 0.94 eV [40]. The results of the high-resolution electron energy loss spectroscopy (HREELS) shown, that two of carbon atoms changed their hybridization from sp^2 to sp^3. This corresponds with change of the benzene to the 1,4 cyclohexadiene-like structure when it is chemisorbed on the surface. Thus the HREELS proved the chemisorption in di-σ-bond bridge position like ethylene. The atomic structure of the chemisorbed benzene can be found on the figures 2.14-2.17. Benzene binds with silicon via two σ bonds: adatom-carbon atom and restatom-carbon atom. Taking into account that the 7×7 reconstruction has four types of the adatoms, there are four inequivalent positions on which benzene can chemisorb. In this work I shall use the following naming convention: If the benzene binds with the *fc* adatom and the restatom then the structure will be called *b-fc*(see figure 2.14). Following the same rule the the *b-fe* (figure 2.15), the uc (figure 2.16)and the *b-ue* (figure 2.17) structures are defined).

The evidence of the di-σ-bridge chemisorption was found by the photoelectron spectrosopy, too [41, 42]. The STM experiments also proved the occurrence of the adatom-carbon σ bond by disappearance of the adatom from STM map. The disappearance is caused by the saturation of the dangling bond that eliminates the state at the Fermi Level located on the adatom [45, 43, 46, 39, 44].

In addition to the experimental evidence, presented above, a number of the-

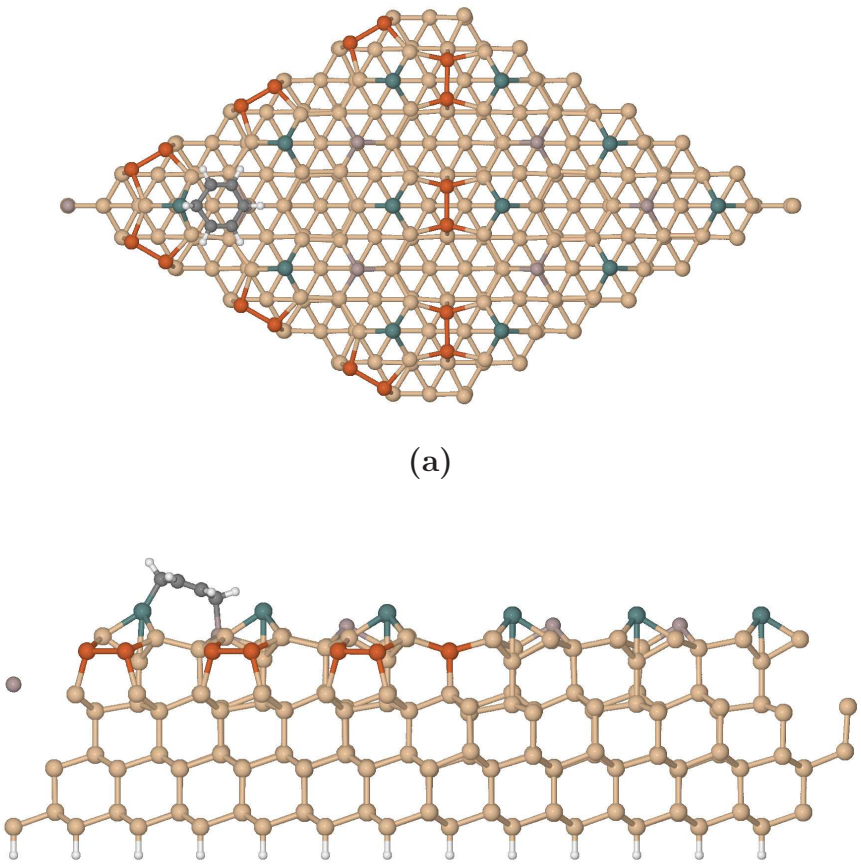

Figure 2.14: *Atomic structure of chemisorbed benzene on 7×7 in di-σ-bridge configuration. So called B-FC structure, due to benzene binds to fc adatom.*:**(a)** *Top view of on 7×7unit cell;* **(b)** *Side view of one 7×7unit cell*

oretical studies confirm the thermodynamically preferred 1-4-di-σ attachment geometry. The majority of the theoretical investigations use Si clusters, that frequently incorporate a single Si rest atom and a single adatom with three or five atomic layers of Si, to model the surface/adsorbate system [47, 48, 49, 50].

In all the above mentioned experiments, there were no real-space observations of the restatom-carbon bond.Also there is a possibility that in the STM experiment, the adsorbed benzene can be mistaken for the adsorbed hydrogen atom on the adatom [51] or the vacant adatom [52].

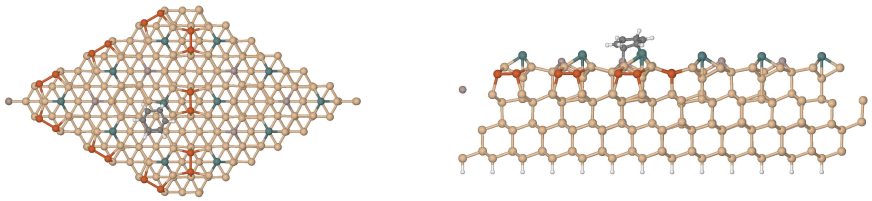

(a) **(b)**

Figure 2.15: *The atomic structure of chemisorbed benzene on 7×7 in the di-σ-bridge configuration. So called B-FE structure, due to benzene binds to fe adatom.:***(a)** *Top view of on 7×7unit cell;* **(b)** *Side view of one 7×7unit cell*

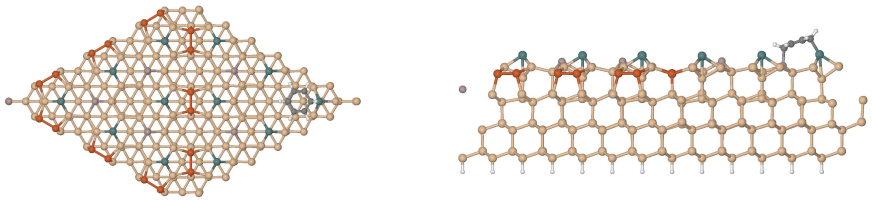

(a) **(b)**

Figure 2.16: *The atomic structure of chemisorbed benzene on 7×7 in the di-σ-bridge configuration. So called B-UC structure, due to benzene binds to uc adatom.:***(a)** *Top view of on 7×7unit cell;* **(b)** *Side view of one 7×7unit cell*

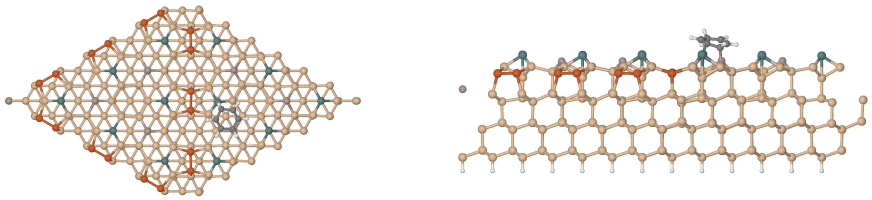

(a) **(b)**

Figure 2.17: *The atomic structure of chemisorbed benzene on 7×7 in the di-σ-bridge configuration. So called B-UE structure, due to benzene binds to ue adatom.:***(a)** *Top view of on 7×7unit cell;* **(b)** *Side view of one 7×7unit cell*

3. STM

3.1 Theoretical introduction

All equations are in SI units.

The scanning tunnelling microscopy (STM) is based on the quantum effect of tunnelling of electrons through a potential barrier, as you can see on the figure 3.1. One of the electrodes, from which (or into which) the electrons are tunnelling, is very sharp metal tip, and second one, into which (or from which) electrons flow is the sample that we want to examine. Direction of the current depends on the applied voltage. The potential barrier between tip and sample is caused by interfaces tip-vacuum and vacuum-sample [53].

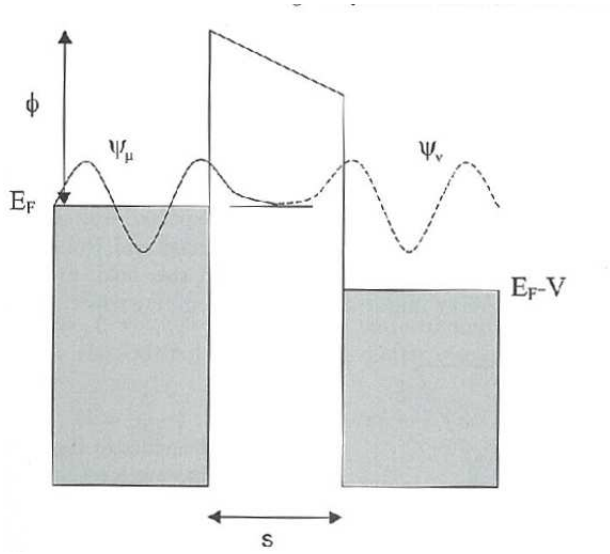

Figure 3.1: *The schematic drawing of one dimensional tunnelling from the tip into the sample, or back. The potential barrier* Φ *mainly depends on the work functions of the sample and the tip, but other effects as screening can affect its height.* Figure taken from E. Meyer, H. J. Hugos and R. Bennewitz [53]

As the initial guess for tunnelling current, when the tip is far away from the sample, the two independent systems can be considered. Then for an independent surface with interface $z = 0$ and with work function Φ the electron wave function $\psi(z)$, located on an energy E, decays exponentially into the vacuum [54]:

$$\psi(z) = \Psi(0) \exp -\frac{\sqrt{2m(\Phi - E)}z}{\hbar}, \tag{3.1}$$

where $\Psi(0)$ is the amplitude of wave function on the interface; m stands for the mass of electron and $\hbar$ is the reduced Planck constant. If the current flows between two identical metal substrates with small applied voltage V between them, and if the density of states (DOS) $\rho(E)$ around Fermi level does not change so much, then simple assumption for tunnelling current I_t can be made that the tunnelling

current depends only on the overlap of the surface wave functions and on the density of states [54]:

$$I_t \sim V\rho(E_F)\exp -2\frac{\sqrt{2m\Phi}z}{\hbar}. \tag{3.2}$$

First experiments with tunnelling current and with well defined gap between the electrodes were made on the metal-insulator-metal tunnelling junctions in 1960. In the same year Bardeen, came up with the time-dependent perturbation approach, which was successfully used for describing a wide variety of effects on them. This approach can be used for a tip-vacuum-sample system, too. Like in the initial guess, the Bardeen approach considers two independent subsystems - the tip and the sample. The tunnelling current between them is calculated by the *Fermi golden rule* [54]:

$$I_t = \frac{4\pi e}{\hbar}\int_{-\infty}^{\infty}[f_s(E_F - eV + \varepsilon) - (f_t(E_f + \varepsilon)]\rho_s(E_f - eV + \varepsilon)\rho_t(E_f + \varepsilon)M^2 d\varepsilon, \tag{3.3}$$

where e is the charge of electron, indexes s and t mean that the quantities are related to the sample and the tip respectively. The Fermi-Dirac $f(E)$ distribution is defined [54]:

$$f(E) = \frac{1}{1 + e^{(E-E_F)/k_bT}}. \tag{3.4}$$

M in eq. (3.3) is the tunnelling matrix obtained by [54]:

$$M = \frac{\hbar}{2m}\int\left(\psi_s^*\frac{\partial\psi_t}{\partial z} - \psi_s\frac{\partial\psi_t^*}{\partial z}\right)dS, \tag{3.5}$$

where the integration goes over whole surface; ψ_s and ψ_t are the wave functions of the sample and the tip respectively [54].

If k_bT is small, in comparison to resolution required in the measurement, than the Fermi-Dirac distribution in eq. (3.3) can be approximated by the step functions. In this case, the tunnelling current can be obtained by [54]:

$$I_t = \frac{4\pi e}{\hbar}\int_0^{eV}\rho_s(E_f - eV + \varepsilon)\rho_t(E_f + \varepsilon)M^2 d\varepsilon. \tag{3.6}$$

Tersoff and Hamann made another approximation of the Bardeen theory. They considered only a s-wave tip. Their approximation results into a simple formula [54]:

$$\frac{dI_t}{dV} \sim \rho_s(E_f - eV), \tag{3.7}$$

which tells us that, for the same height of the tip above the surface and for the constant voltage, the current depends only on a local density of states (LDOS) of the sample [54].

For the STM simulations in this work I will use the STM code, which is described by Blanco et al. [55]. This code is based on the improved Bardeen approach.

The main problem of the original Bardeen approach is the bad decay of tunnelling current in far distance, because of the assumption of the square barrier between the sample and the tip [55]. In the STM code the barriers for the tunnelling between different orbitals of atoms are pre-calculated by Fireball. In these

pre-calculations a basis set with big radial cuts (see chapter 1.4) are used. These barriers are then used for computing matrix elements of M.

Also, when high voltages are used, the electrons can tunnel from different energy states. The tunnelling barrier is different for the states near the Fermi Level and for the states far away from it. Thus, these changes of the barrier can be approximated by exponential damping. The height of the barrier $\Phi(\varepsilon)$ then will be varied with the energy ε [55]:

$$\Phi(\varepsilon) \sim \Phi_0 e^{-\frac{\varepsilon}{W}}, \tag{3.8}$$

where Φ_0 is the height of the barrier on the Fermi Level and the energy window W is an empirical parameter. When this exponential damping is substituted into eq. (3.6), then the tunnelling current is obtained by [55]:

$$I_t = \frac{4\pi e}{\hbar} \int_0^{eV} \rho_s(E_f - eV + \varepsilon)\rho_t(E_f + \varepsilon)M^2 e^{-\frac{\varepsilon}{W}} d\varepsilon. \tag{3.9}$$

The STM code uses eq. (3.9) for calculations of tunnelling current.

3.2 The technical solutions and operational modes of a STM

The experimental arrangement of any STM consists of three mutually perpendicular piezoelectric transducers. If the voltage is applied on them, they will move with the tip in x,y and z direction above the studied sample. The sample must be fixed in such position so the x and y movements of the piezo-positioners are parallel with the surface (as much as possible). A very sharp probe tip is often made from W or Pt-Ir alloy by the electrochemical etching. To obtain atomic resolution the whole STM system has to be isolated from vibrations. Depending on a particular arrangement, the STM can work in different ambiences: in air, in inert gas, in liquids and ultra high vacuum (UHV). The operating temperature can be also varied depending on type of STM used. The low temperature STM works in temperatures around absolute zero, while the high temperature STM works in few hundred degrees of Celsius [54].

So far, there are a couple of operational modes in which STM can work:

In the *constant height mode* is the height of the tip maintained during whole measurement. The information obtained from the experiment is the tunnelling current - $I(x, y)$. This operational mode is not very popular, because there is the possibility that the tip can crash into a bumps on the surface [54].

The most common STM mode is *constant current mode*. In this mode the required current is maintained by feedback loop. The loop is changing the height of the tip above the surface, which is the measured quantity - $z(x, y)$ [54].

While working in the *constant height mode*, it is possible to gain local density of states (LDOS) in so called *dI/dV mode*. In this mode the LDOS is obtained by using eq. (3.7). The derivation can be made experimentally by lock-in amplifier, if high frequency oscillations of voltage are used. For more details see [36].

Quasi constant height mode bypasses the problems with the crashing of the tip into the sample by applying a small amount of feedback, that responds to the average current. As the topographic height of the surface increases, the

tunnelling current is also significantly bigger and therefore the tip slowly moves further from the surface. Also, when the height of the surface decreases then the current decreases for some time and the tip moves towards the surface. This circumstances lead to shadowing effect of bigger structures as islands, that is typical for the *quasi constant height mode* [56].

4. Results and discussion

4.1 Experiment - the $\sqrt{3} \times \sqrt{3}$ reconstructions

All the stated bias voltages are applied to the sample.

The experiment made by Dr. Pavel Kocán. started with the 7×7 reconstructed Si (111) surface on which one monolayer of thallium was adsorbed in order to cancel the 7×7 reconstruction. The result of the adsorption of Tl was a bulk terminated-like silicon substrate with Tl in T_4 adatom position. But the structure of the silicon was not ideal due to some remaining borders of the original 7×7 cells. After heating the sample up to 350 °C the thallium desorbs. When the sample was heated up to the 450 °C then LEED showed that the surface was chiefly 2×1 *Pandey chain* reconstructed, but some small areas were $\sqrt{3} \times \sqrt{3}$ $R30°$ reconstructed. After following heating the portion of $\sqrt{3} \times \sqrt{3}$ reconstruction started to grow. If the temperature of the sample reached 550 °C then almost the whole surface was $\sqrt{3} \times \sqrt{3}$ $R30°$ reconstructed. On the other hand after reaching temperature 600 °C the surface was reconstructed only 2×1 *Pandey chain*. If the surface was heated up to temperature higher than 650 °C then the transition to 5×5 DAS and later to 7×7 DAS reconstruction was observed. The changes in portions of reconstructions observed by LEED can be seen in the figure 4.1. This whole procedure was repeated many times and its results were fully reproducible.

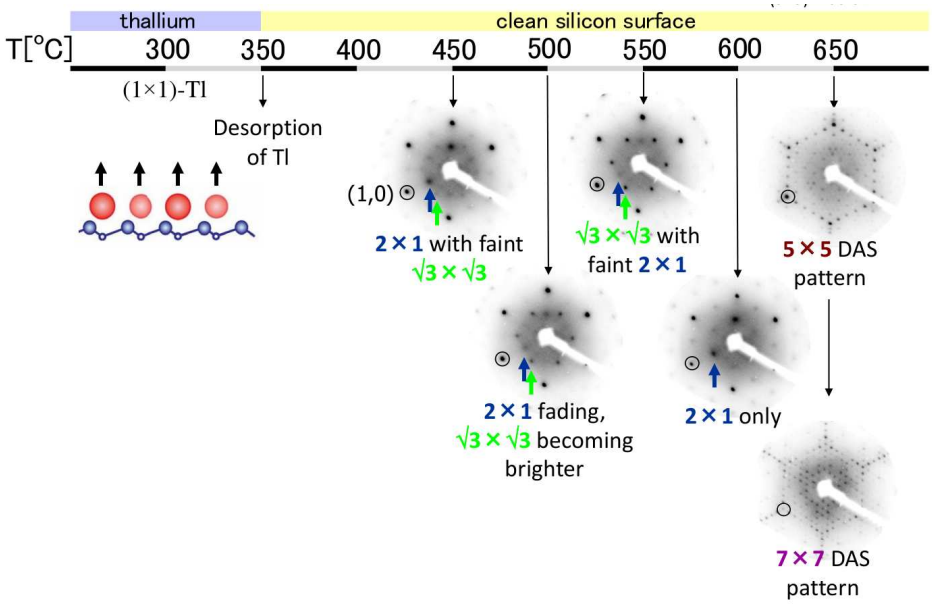

Figure 4.1: *Structural changes of the Si (111) surface observed by LEED.*

The STM map of the surface with coexisting $\sqrt{3} \times \sqrt{3}$ and 2×1 phases can be found in the figure 4.2. The line profiles (see figure 4.3) proved, that the observed $\sqrt{3} \times \sqrt{3}$ reconstruction was not the *adatom* reconstruction, because the *adatom* reconstruction has the highest atom located about 1 Åabove the highest of the 2×1 *Pandey chain* reconstruction. In the experiment the maximal measured

height of the tip above the vs reconstruction was lower than the maximal height of the tip measured above the 2×1 *Pandey chain* reconstruction.

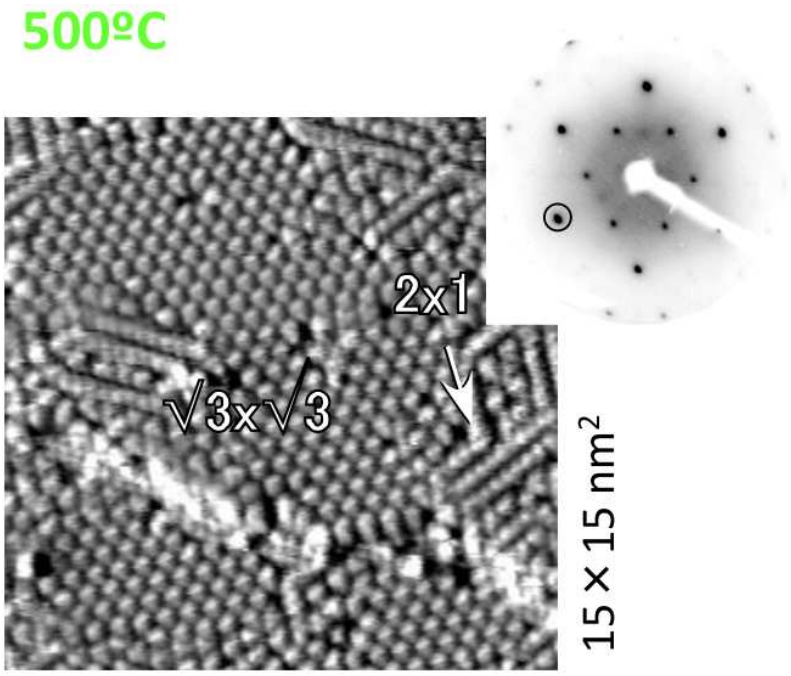

Figure 4.2: *The STM map of Si (111) surface showing areas with* $\sqrt{3} \times \sqrt{3}$ *and 2×1 Pandey Chain reconstructions. The map was obtained at room temperature in the quasi-constant height mode with applied bias voltage + 2.0 V. The maximal temperature reached during heating of the surface was 500 °C. The LEED pattern of the surface is in top right corner.*

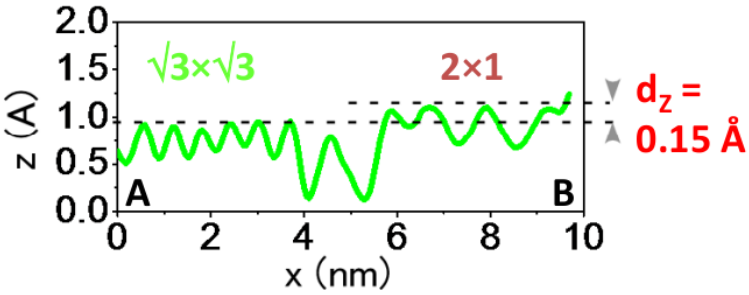

Figure 4.3: *STM constant current line profile of Si (111) surface taken above areas reconstructed* $\sqrt{3} \times \sqrt{3}$ *and 2×1 Pandey Chain. The bias voltage was + 1.5 V.*

In the section 4.3.2 the possible structure of this unknown $\sqrt{3} \times \sqrt{3}$ $R30°$ reconstrucion will be discussed.

4.2 Experiment - Benzene on the 7×7 DAS

The experiment bearing on the chemisorption of benzene on 7×7 DAS was performed by Prof. Alastair McLean. The submonolayer of benzene was evaporated onto 7×7 reconstructed clean silicon surface via the precision leak valve at room temperature. After that STM observations of the surface were done at room temperature. The chemisorbed benzene was found in all the mentioned di-σ-bridge positions - *b-fc*, *b-fe*, *b-uc* and *b-ue* (see figure) 4.5. From the figure 4.5 you can see, that the chemisorption of benzene causes disappearance of binded adatom from the STM maps in empty states of the sample (positive bias voltages) as well as in filled states (negative bias voltages). However, in filled states there can also be seen significant increase of brightness of adatoms closest to the adsorbed benzene. This feature will be discussed later.

Simultaneously with the STM maps, the dI/dV maps were measured in order to find an evidence of the restatom-carbon atom bond. The STM and dI/dV map of the area with at least four adsorbed benzenes can be found in the figure 4.4. The dI/dV map proved the presence of the restatom-carbon atom bond by the disappearance of the restatom in the map.

These features mentioned above will be explains by means of the DFT calculations and the STM simulations in the chapter 4.3.3.

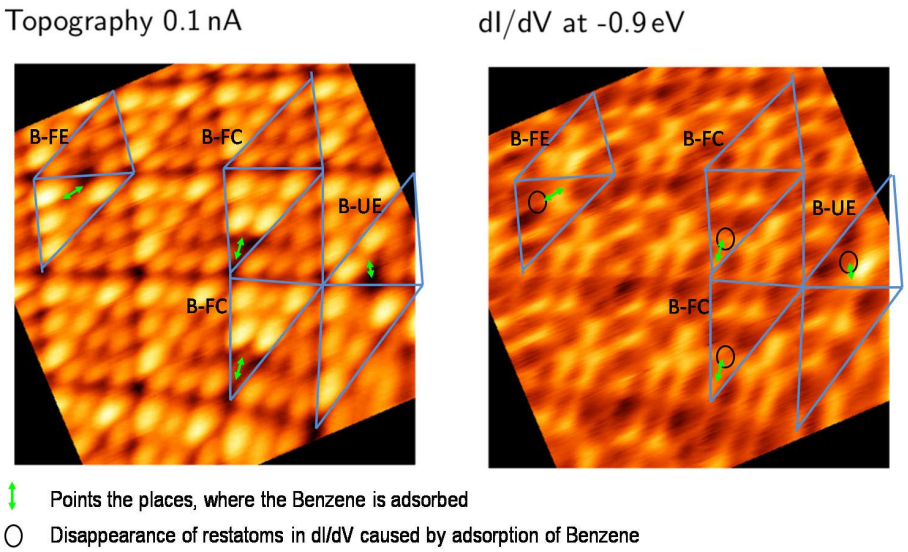

Figure 4.4: *The constant current map of the 7×7 reconstructed Si (111) surface with the chemisorbed benzene on it in different adsorption positions (left). The dI/dV map of the same area (right). Both the STM and dI/dV maps were taken with applied bias voltage - 0.9 V, The positions of the benzenes are marked by the green arrows. The black circles in dI/dV mark disappearance of the restatoms due to the σ bond with a carbon atom of the benzene.*

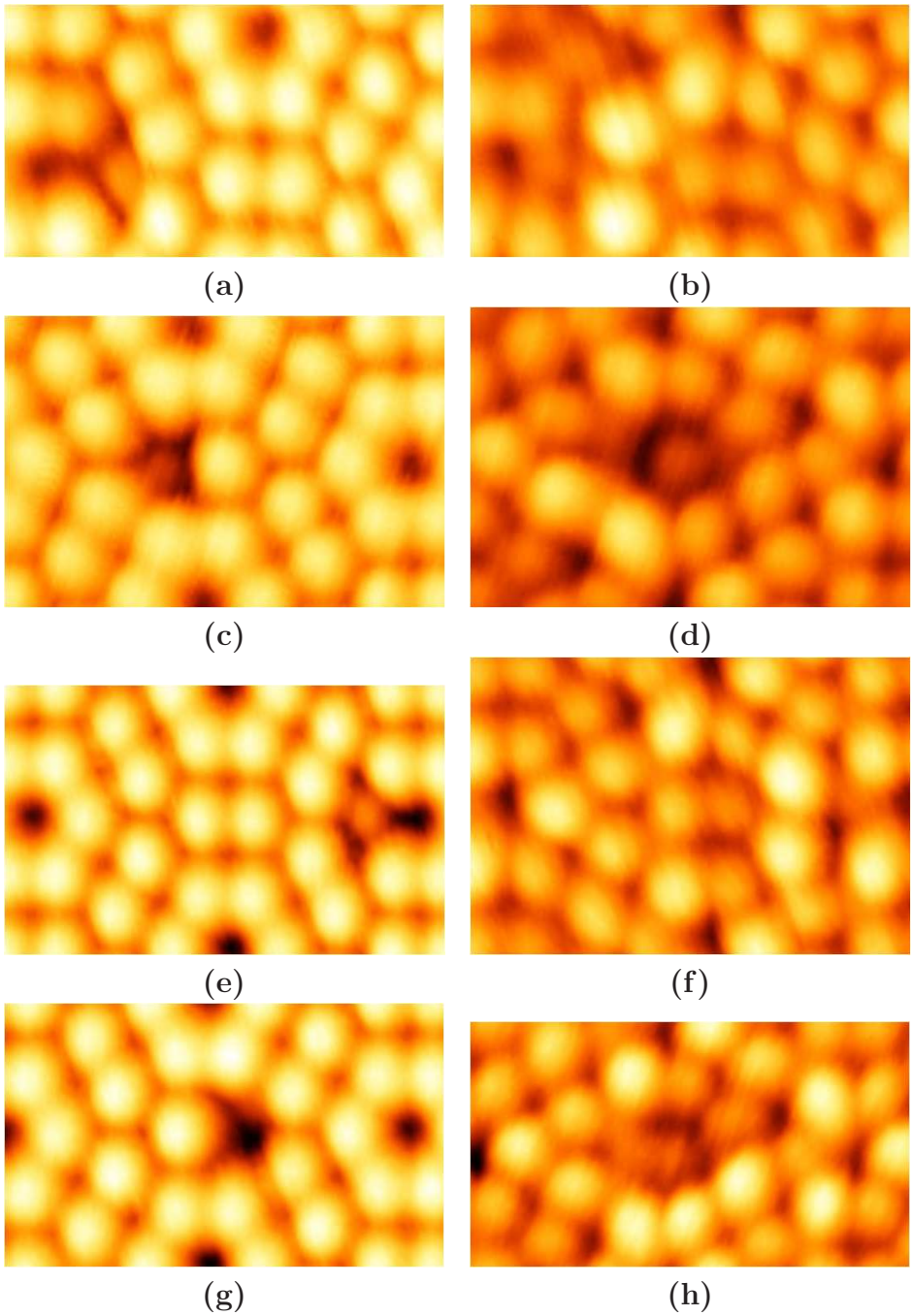

Figure 4.5: *The STM constant current figures of the benzene adsorbed on 7×7for bias voltage + 0.6 V (left column) and bias voltage - 0.6 V (right column). The benzenes are adsorbed in different positions*: **(a)**, **(b)** *Benzene in position b-fc;* **(c)**, **(d)** *Benzene in position b-fe;* **(e)**, **(f)** *Benzene in position b-uc;* **(g)**, **(h)** *Benzene in position b-ue.*

4.3 Theoretical calculations

4.3.1 Introduction

All my DFT calculations were made with the Fireball code and with usage of the norm-conserving pseudopotentials, thus only the valence electrons were taken into account. For all my calculations I used the basis sets of s and s^* orbitals for H, s,p and d orbitals for C and s,p and d orbitals for Si. The radial cuts of the orbitals are in the table 4.1. The basis set and pseudopotentials give us the total energy of a single silicon atom in a vacuum as 99.98 eV and a single silicon atom in the bulk as 106.67 eV. The computed ideal lattice constant of the crystalline Si is slightly longer, than the real value - 5.48 Å from the calculation vs. 5.43 Å from the experiment [13]. This difference causes, that sizes and distances in this work can be slightly bigger than in an experiment or other calculations.

All the Si (111) slab calculations were made with total eight layers of silicon, passivated by one layer of hydrogen underneath, in order to prevent problems caused by the remaining dangling bonds on the bottom of the slab. There were used 3D periodic boundaries with $\sim$ 90 Å of the vacuum between the individual slabs. For the Brillouin zone sampling the Monkhorst-Pack grid method [57] was used. I used 64 k-points for the 1×1 unit cell, 32 k-points for the 2×1 unit cell, 16 k-points for the $\sqrt{3} \times \sqrt{3}$ $R30^\circ$ unit cell and 4 k-points for the 7×7 unit cell. By means of additional total energy calculations with more k-points than mentioned above I made sure that the number of k-points was sufficient.

Table 4.1: *Radial cuts r_c of the orbitals in the used basis set.*

Atom	Orbital	$r_c[a_b]$
H	s	3.8
	s∗	3.8
C	s	4.0
	p	4.5
	d	5.4
Si	s	4.8
	p	5.4
	d	5.6

a_b - Bohr radii: $a_b = 0.529$ $\mathring{A}$.
$*$ - excited orbital.

All my simulations of STM maps were done in the constant current mode, which is much easier to compute. For these simulations I have used a pyramidal tungsten tip with single atom on its top. The atomic structure and the density of states of the tip can be seen in the figure 4.6. Because the approach of the STM code is only approximative and it does not take into account the resistivity of the sample and the tip, the STM maps cannot be reproduced quantitatively, they can be reproduced only qualitatively. Therefore the current range is not shown in the simulated STM maps.

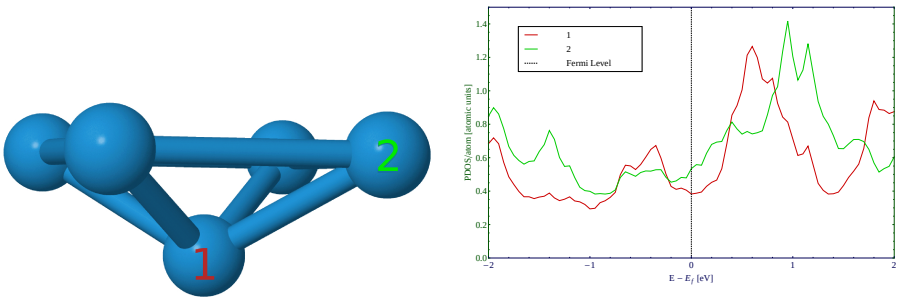

(a) **(b)**

Figure 4.6: **(a)** - *The atomic structure of the apex of the tungsten tip used for STM simulations.* **(b)** - *The PDOS of the apex atoms of the tip.*

4.3.2 Si (111) reconstructions

4.3.2.1 Energetic favourableness of studied reconstructions

For the comparison of reconstructions of Si (111) surface I made total energy calculations of the reconstructions I wanted to compare. Namely it were relaxed the bulk terminated surface (*1×1 relaxed* for short), the nonrelaxed bulk terminated surface (*bulk terminated* for short), the left-chain isomer of 2×1 *Pandey chain* (*2×1-l*), the right-chain isomer of 2×1 *Pandey chain* (*2×1-r*), the $\sqrt{3} \times \sqrt{3}$ $R30°$ vacancy (*vacancy*), the $\sqrt{3} \times \sqrt{3}$ $R30°$ T_4 adatom (*adatom*), the 7×7 DAS (7×7) and two different structures of the $\sqrt{3} \times \sqrt{3}$ $R30°$ buckled reconstruction and one new $\sqrt{3} \times \sqrt{3}$ $R30°$ reconstruction that I called a *Pandey like*, which will be discussed later (see chapter 4.3.2.3). The *buckled* reconstructions differ in the arrengement of the first layer: the *buckled* (1) reconstruction has one up atom and two down atoms, while the *buckled* (2) has two up atoms and two down atoms.

The comparison of the energetic favourableness according to the eq. (2.1) of all the mentioned reconstructions can be found in the table 4.2 and the graphical comparison (for the most interesting of them) can be found in the figure 4.7. If there are no extra atoms or vacancies in the reconstructions, then the comparison of their energetic favourableness can be made by comparing their normalized total energies - $E^{TOT}_{n\times m}/(n \times m)$. This concerns the *bulk terminated*, the *1×1 relaxed*, the *2×1-r*, the *2×1-l*, the *buckled* (1),the *buckled* (2) and the *Pandey like* reconstructions. If there are some extra atoms or vacancies, then the eq. (2.1) hat to be used. The only unknown parameter in the eq. (2.1) is the chemical potential of the silicon μ. The atoms on the surface are not bound so strength as in the bulk, but on the other hand the energy of the Si at. in the vacuum is probably far away from the true value, because every atom on the surface has at least three neighbours. Thus assumptions that the chemical potential is somewhere near the energy of the Si at. in the bulk (-106.67 eV) can be made.

From the table 4.2 and from the figure 4.7 you can see, that if the chemical potential μ is around energy of Si at. in bulk, then the 7×7 is the most favourable reconstruction, which is in the good agreement with other theoretical calculations eg. [32, 24] and experimental observations [22].

Table 4.2: *Energetic comparison of the calculated reconstructions.*

Reconstruction	$E^{TOT}_{n\times m}[eV]$	$\frac{E^{TOT}_{n\times m}}{n\times m}[eV]$	$\frac{N_{n\times m}}{n\times m} - N_{1\times 1}$	$\alpha(\mu = -106.67eV)[eV]$
bulk terminated	-866.51	-866.17	0	0.00
1×1 relaxed	-866.66	-866.66	0	-0.49
2×1-r	-1733.70	-866.84	0	-0.68
2×1-l	-1733.68	-866.84	0	-0.67
vacancy	-2492.95	-830.98	-1/3	-0.37
adatom	-2707.49	-902.50	1/3	-0.77
buckled (1)	-2600.32	-866.77	0	-0.61
buckled (2)	-2600.09	-866.70	0	-0.54
Pandey like	-2600.36	-866.79	0	-0.62
7×7	-42914.72	-875.81	4/49	-0.93

The second most stable reconstruction is the *adatom* reconstruction. The reason why this reconstruction was not much observed is probably in the reconstruction kinetics. The experiment made by Minoda et al. [31] probably moved the chemical potential to the higher energies, by means of evaporating silicon onto the surface, and therefore they got to the energy areas where the *adatom* reconstruction is the most stable.

The stability of the 2×1 *Pandey chain* was already discussed in the chapter 2.3.1. The *buckled* and the *Pandey like* reconstructions and their stability will be discussed in the chapter 4.3.2.3.

On the other hand, the *vacancy* reconstruction was even less stable than just relaxed surface. So this reconstruction is unlikely to appear on the surface unless the surface is subjected some special procedure like ion bombardment, like it was in the experiment of Fan et al. [30].

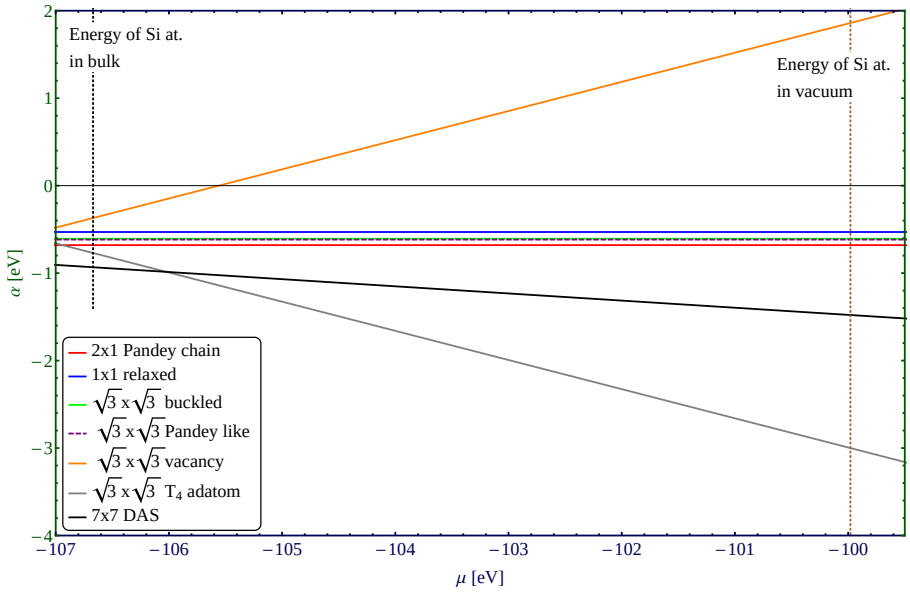

(a)

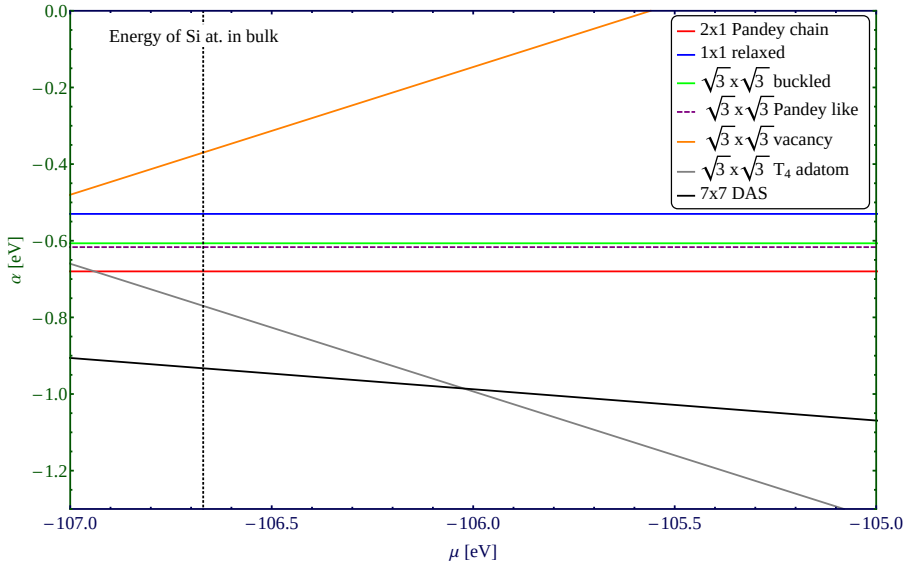

(b)

Figure 4.7: *The comparison of energetic favourableness of studied reconstruction of Si (111) depending on the chemical potential of Si at.* μ: **(a)** *Dependence of the favourableness on the chemical potential, for all the possible values of the chemical potential;* **(b)** *Detail of the dependence for the chemical potential near the energy of Si in the bulk.*

4.3.2.2 The 2×1 *Pandey chain*

My total energy calculations also proved, that the *2×1-l* is more favourable than the *2×1-r*. But the energetic difference between the *2×1-l* and the *2×1-r* was slightly higher than in the calculations of Garlef et al. [26] and Stekolnikov et al. [24]. The difference calculated by myself is 0.15 eV. The calculations showed that a gap of the *2×1-l* is 0.5 eV, which is more than in the mentioned calculations (0.3 eV) and the height difference between up atom and down atom is much bigger - 0.75 Å vs. 0.63 Å taken from calculations of Stekolnikov et al. My results of the *2×1-r* reconstruction assign bigger height difference between up atom and down atom, too. The height difference calculated by me is 0.7 Å vs. approximately 0.5 Å from calculations of Garlef et al. [26] and Stekolnikov et al. [24]. From my previous calculations [4] I know, that the Fireball code gives a quite larger buckling and height differences, than other computations. On the other hand the calculated gap of the *2×1-r* - 0.6 eV - was in quite good agreement with previous calculations [26, 24] - 0.7 eV. The partial density of states per atom (PDOS) for the topmost atoms for both isomers of the 2×1 *Pandey chain* is shown in the figure 4.8.

The bigger height difference between the up and the down atom might be the reason why I did not manage to reproduce the STM maps for the low positive voltages (empty states). The experiments and calculations of Garlef et al. show the down atoms as the bright protrusions, however in my calculations the up atoms are the brightest in all simulated voltages. The only exception is the simulation with the applied voltage + 0.5 V, where the whole chain looks equally bright (see figure 4.9). I made simulations of both 2×1 *Pandey chain* isomers, in this work only the results for the *2×1-r* are shown, because its gap is much closer to the experimental observations [26]. The difference might be also caused by usage of tungsten tip for the STM simulations. Garlef et al. [26] used Tersoff-Hamann approximation only. In the experiment there is no chance how to examine the apex of the tip. The Fermi level in the experiment can differ from the calculations. The reason for this is that the examined samples in the experiment are doped with other elements.

The difference of the gaps and the row directions in the low voltage-STM simulations between my calculations and the calculations of Garlef et al. can be caused by the fact that Garlef et al. used much more precise method for the electronic structure calculations [26].

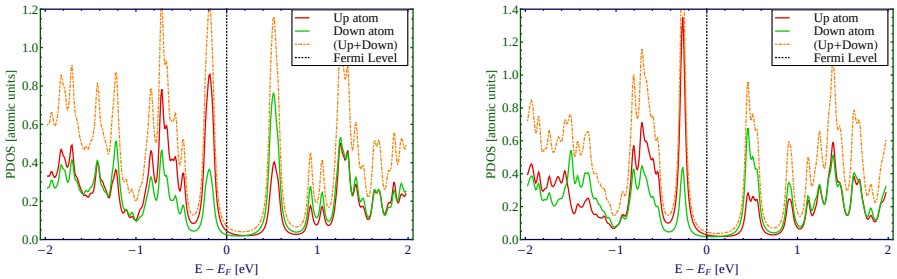

(a) **(b)**

Figure 4.8: *Density of states of the up atom and the down atom of the 2×1-l* **(a)** *and the 2×1-r* **(b)**.

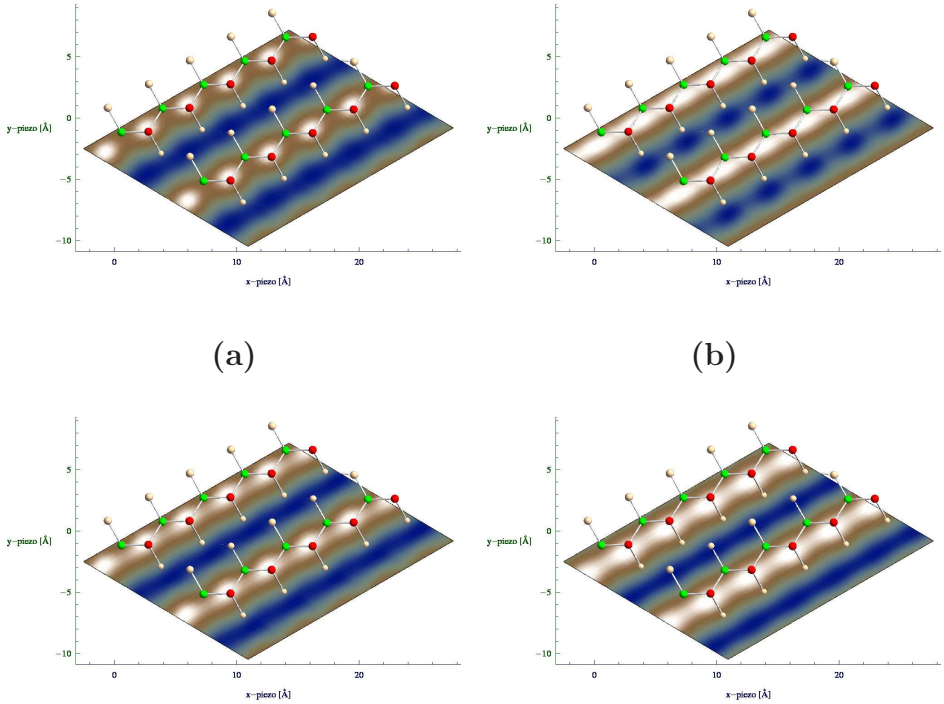

(a) **(b)**

(c) **(d)**

Figure 4.9: *Constant height STM simulations of the* 2×1-r *reconstructed Si (111) surface for bias voltage:* **(a)** *- 0.5 V,* **(b)** *+ 0.5 V,* **(c)** *+ 1.0 V, and* **(d)** *+ 1.5 V. The height of the tip was 5 Å above the up atom. The up atoms are red, down atoms are green.*

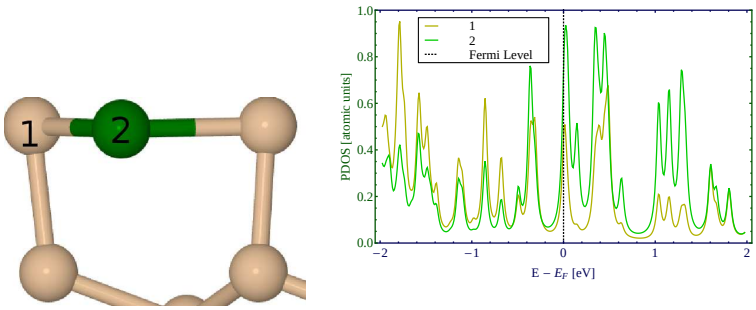

(a) **(b)**

Figure 4.10: *The vacancy reconstruction:* **(a)** *legend for the PDOS.* **(b)** *the PDOS of the topmost atoms.*

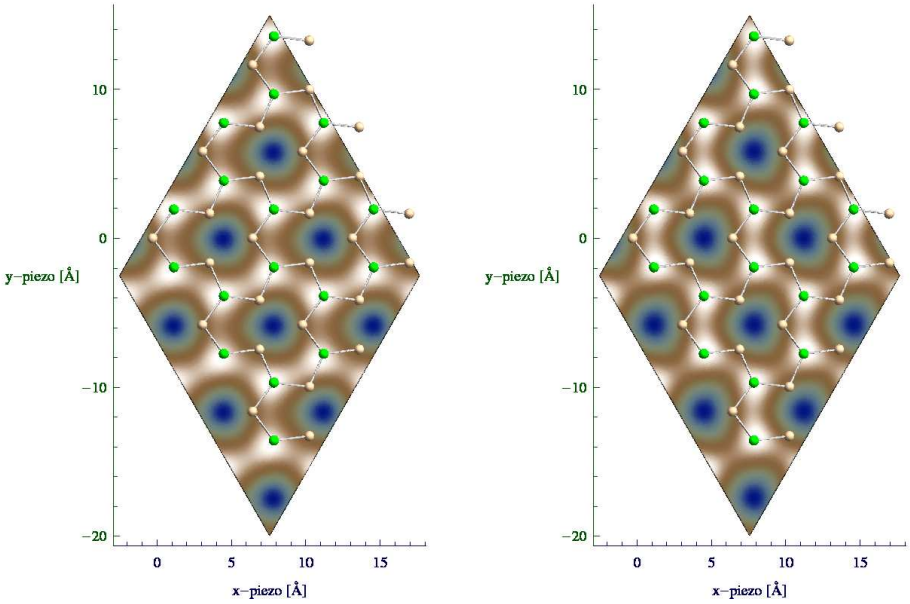

(a) **(b)**

Figure 4.11: *Constant height STM simulations of the* vacancy *reconstructed Si (111) surface for bias voltage:* **(a)** *+ 1.5 V,* **(b)** *+ 1.8 V.*

4.3.2.3 The $\sqrt{3} \times \sqrt{3}$ $R30°$ reconstrucions

For each of the $\sqrt{3} \times \sqrt{3}$ $R30°$ reconstructions I will show simulations of the high positive bias voltages only, because they can be compared with the experimental data obtained by Dr. Pavel Kocán. The height of the tip in the simulations was specified 4.0 Å above the up atom of the *buckled* (1) reconstruction. This means that height of the tip in the simulations was 5.2 Å above the top of *vacancy* reconstruction, 3.1 Å above the *adatom* reconstruction and 4.0 Å above *Pandey like* reconstruction. The height of the tip was estimated this way in order to simulate the experimental data observed by Dr. Pavel Kocán. as realisticly as possible.

The simulations of the *vacancy* reconstruction showed, that the remaining two topmost atoms moved down onto the level of the atoms of the second layer during the relaxation - green atom no. 2 in the figure 4.10 **(a)**. By this shift

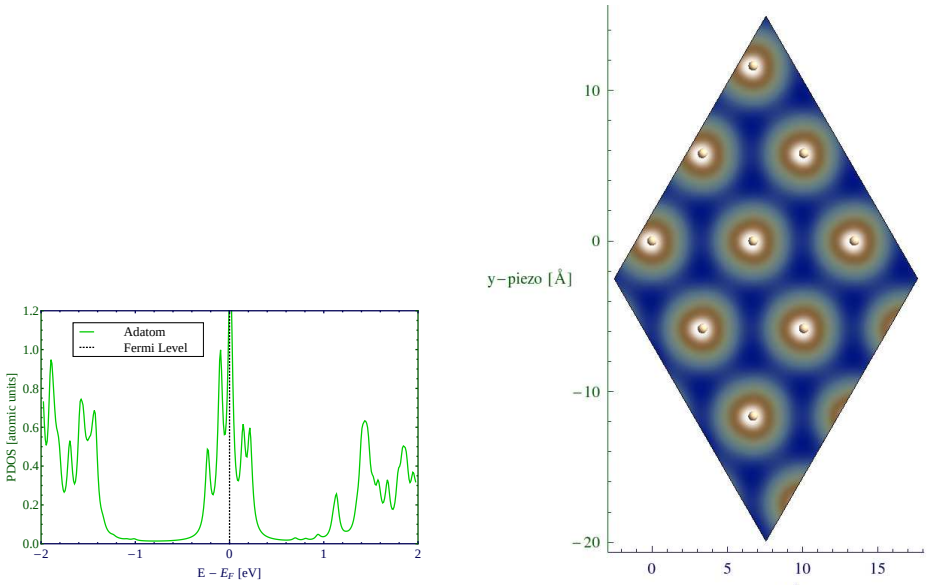

(a) **(b)**

Figure 4.12: *The adatom reconstruction:* **(a)** *the PDOS of the adatom.* **(b)** *The STM simulation with applied bias voltage + 1.5 V. Only the positions of the adatoms are shown.*

they changed their hybridization from sp^3 to sp^2. The atoms near vacancy moved 0.4 Å towards the missing atom. On the PDOS in the figure 4.10 you can see, that this reconstruction has states on the Fermi Level and there is not big difference between the two types of atoms of the topmost layer in the PDOS.

The STM simulations of the *vacancy* reconstruction can be seen in the figure 4.11. As you can see, STM simulations show positions of the atoms of the topmost layer with the same brightness independently on the type of atom. The lack of contrast in STM simulations is caused by the lack of distinctive differences in PDOS.

The results of calculations concerning the *adatom* reconstruction did not show anything unexpected. The adatom sits in T_4 position 2.66 Å above the the atom of second layer. The height difference between the adatom and the atoms of the first layer is 1.45 Å. The PDOS of the adatom (see figure 4.12 **(a)**) shows states on the Fermi level caused by the dangling bond. The states far from the Fermi level can be assigned to the backbonds between adatom and atoms of the first layer. The STM simulations for any applied voltage show just adatoms. That is because of the dangling bond situated on the adatom and because of the height difference between the adatom and other atoms. In the figure 4.12 **(b)**) is shown the simulation for applied bias voltage + 1.5 V.

The *buckled* (2) reconstruction is much more energetically unfavourable in comparison to the *buckled* (1) reconstruction. Thus in this work I will focus only on the *buckled* (1) reconstruction. The relaxation of the atomic structure ended with the up atom 0.7 Å higher than in the case of the relaxed bulk terminated surface. The down atoms moved 0.5 Å down almost onto the height level of the atoms of the second layer during relaxation, therefore they changed their hybridization to sp^2, as in the case of the *vacancy* reconstruction. Together with

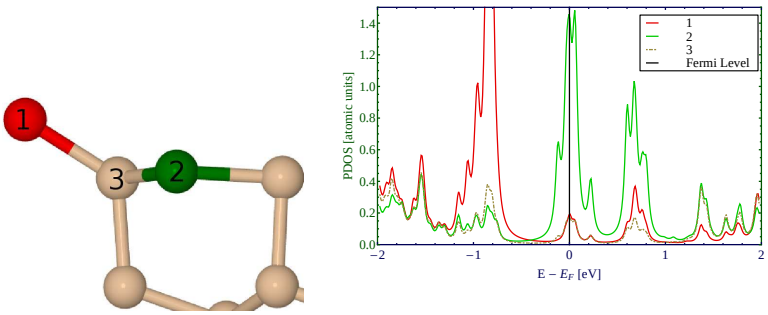

(a) (b)

Figure 4.13: *The buckled reconstruction:* **(a)** *legend for the PDOS.* **(b)** *the PDOS of the topmost atoms.*

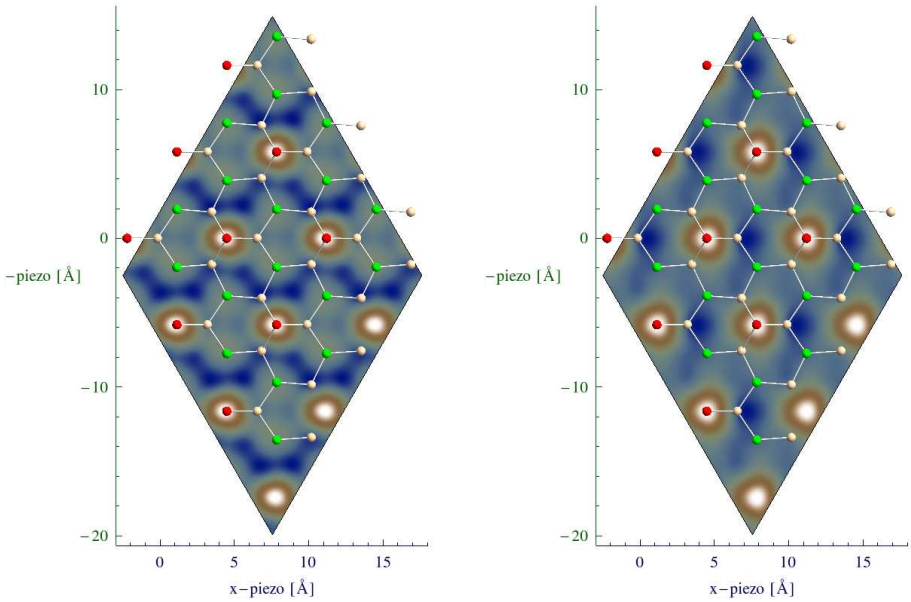

(a) (b)

Figure 4.14: *Constant height STM simulations of the* buckled *reconstructed Si (111) surface for bias voltage:* **(a)** *+ 1.5 V,* **(b)** *+ 1.8 V.*

the changes in the atomic structure also some charge transfer appeared. One electron from the down atoms fully saturates the dangling bond located on the up atom. So there are no states on the Fermi Level located on the up atom. The down atoms with one non-pair electron, cannot directly interact with each other so they have states on the Fermi level, as you can see in the figure 4.13. The comparison, with calculations of F. Ancilotto et al. [33] showed a buckling of 0.9 Å in contrast with my results - 1.2 Å. This overestimation was already discussed. In the densities of states you can see, that the state on the up atom is situated somewhere around - 1.0 eV in my calculations, in comparison to - 0.5 eV from the calculations of F. Ancilotto et al. This difference can be caused by the different buckling or different *exchange-correlation* functional or basis set. F. Ancilotto et al. [33] did not write out details about used method.

Although there are almost no empty states located on the up atom, since the

calculated height difference between up atom and down atom is 1.2 Å the up atom is the brightest in the STM simulations in empty states. But as you can see in the figure 4.14 the down atoms are seen as less bright protrusions in the simulations.

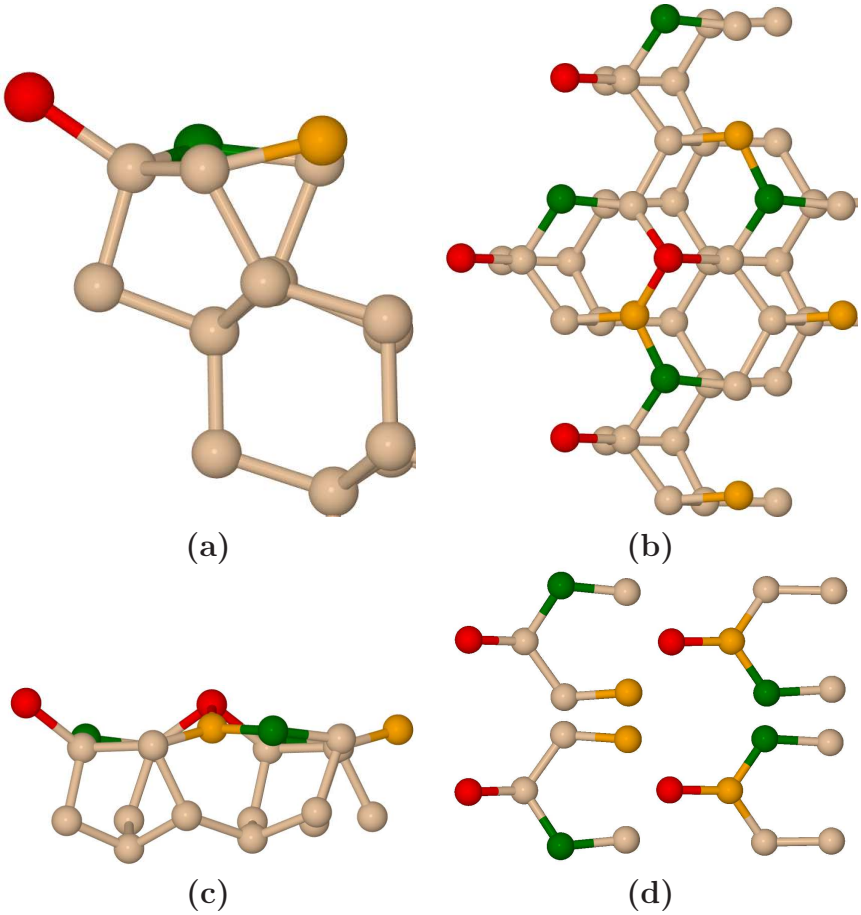

Figure 4.15: *The Pandey like reconstruction:* **(a)** *Side view of one unit cell;* **(b)** *Top view of four unit cells;* **(c)** *Side view of two unit cells showing five member and seven member ring, that can be observed in the first four layers;* **(d)** *Four isomers of the Pandey like reconstructions.*

Because the results of the *buckled* reconstruction are in a quite good agreement with the experiment I made also dynamic simulations at room temperature in order to find out if this reconstruction is stable. But these simulations showed me even more favourable reconstruction. In the simulations the *buckled* reconstruction turned almost immediately into structure, which I called *Pandey like*. This reconstruction can be seen in the figures 4.15. I called this reconstruction *Pandey like* because there are five and seven member rings from side view (as you can see in the figure 4.15 **(c)**), which are typical for 2×1 *Pandey chain* reconstruction. The *Pandey like* developed from *buckled* by exchange of one bond between atoms of the third and second layer into new bond between the same atom of third layer and down atom. This exchange of bonds leaves one atom of second layer (the orange one on figure 4.15) with only three bonds. This atom changes its hybridization from sp^2 to sp^3 and makes double bond with neighbouring down atom. The double bond leads into small gap as you can see in the

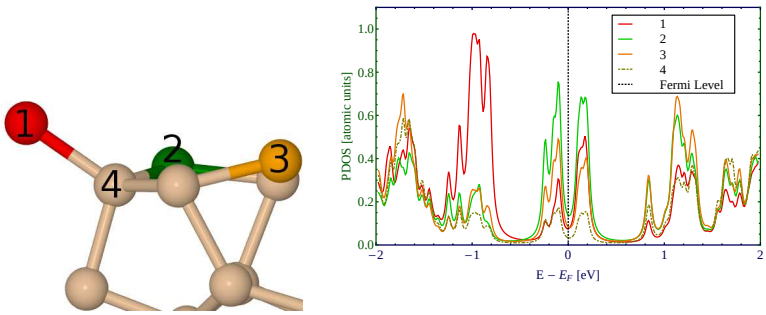

(a) **(b)**

Figure 4.16: *The Pandey like reconstruction:* **(a)** *legend for the PDOS.* **(b)** *the PDOS of the topmost atoms.*

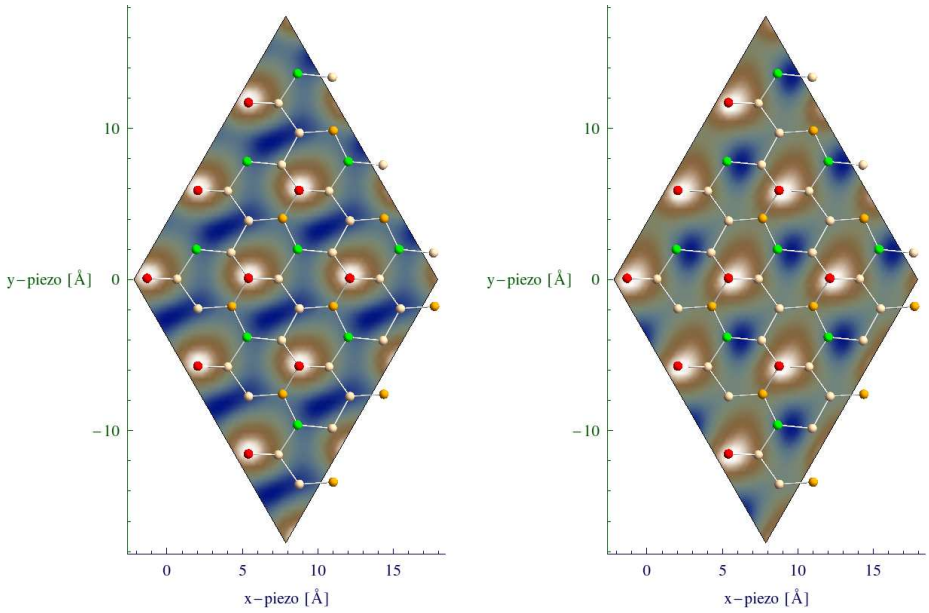

(a) **(b)**

Figure 4.17: *Constant height STM simulations of the* Pandey like *reconstructed Si (111) surface for bias voltage:* **(a)** *+ 1.5 V,* **(b)** *+ 1.8 V.*

figure of PDOS of the structure 4.16. The elimination of states on the Fermi level makes this reconstruction more favourable than the *buckled* reconstruction.

As you can see in the figure 4.17 the changes in the geometry, that make the structure less symmetrized than the *buckled* reconstruction, make less symmetrized also its STM simulations. On the other hand these simulations do not differ so much from the simulations of the *buckled* reconstruction.

The dynamic simulations at room temperature showed that this reconstruction changes its isomerization. During the simulation the up atom did not change its position, while the down atom, the orange atom on figure 4.15 and atom of second layer changed their positions once in approximately 5 ps. All four possible isomers are shown in the figure 4.15 **(d)**. The transition state between two isomers of the *Pandey like* reconstruction is the *buckled* reconstruction. That means, that the barrier of the change of isomerization is about 0.47 eV.

Taking into account the dynamical changes of isomerization, I simulated the STM at room temperature (RT) by averaging current from all the isomers. The resulting STM maps are much more symmetrized, as you can see in the figure 4.18. These maps differ from simulations of buckled geometry. In the RT simulations of *Pandey like* reconstruction are bright only up atoms only and there are no traces of other atoms in them.

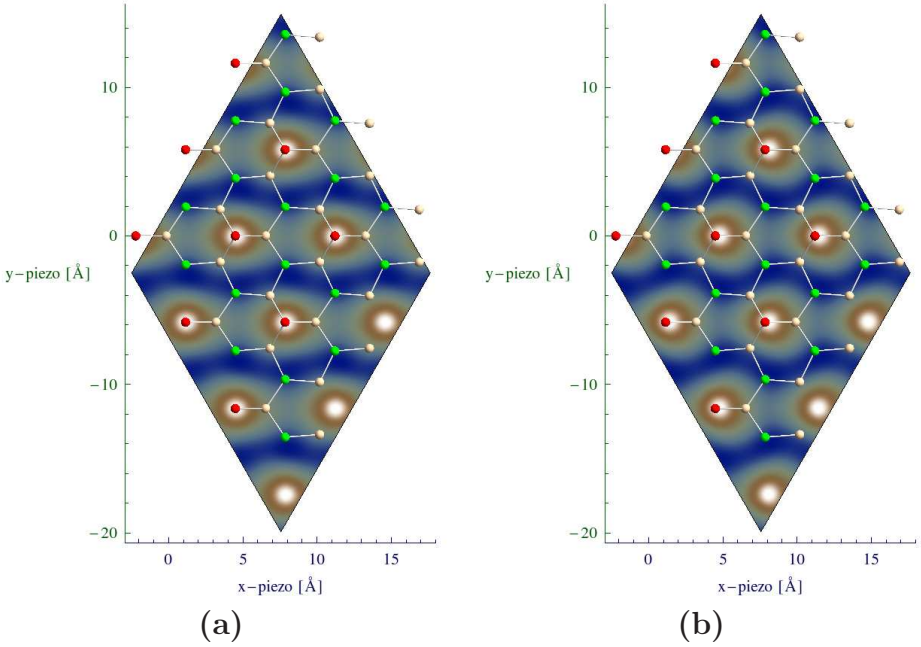

Figure 4.18: *Constant height room temperature STM simulations of the* Pandey like *reconstructed Si (111) surface for bias voltage:* **(a)** *+ 1.5 V,* **(b)** *+ 1.8 V. The current was obtained by averaging current from STM simulations of all* Pandey like *isomers. The shown geometry of the* buckled *reconstruction is just for better orientation.*

4.3.2.4 The $\sqrt{3} \times \sqrt{3}$ reconstructions - comparison with the experiment

The proof that the observed $\sqrt{3} \times \sqrt{3}$ reconstruction is not the *adatom* reconstruction was already mentioned in the chapter 4.1. The line profile, which was lower above the $\sqrt{3} \times \sqrt{3}$ reconstructed area than above the 2×1 *Pandey chain* reconstructed area, does not correspond to the atomic and the electronic structure of the *adatom* reconstruction. The *adatom* reconstruction has the highest atom about 1 Å higher than 2×1 *Pandey chain* , and it also has the dangling bond, which induced high current. To estimate the maximum height of the line profile I calculated maximal current for all the $\sqrt{3} \times \sqrt{3}$ reconstructions and *2×1-r* reconstruction with the constant height of the tip (see table 4.3). The maximal current for the *adatom* reconstruction is one order of magnitude higher than maximal current for the *2×1-r* reconstruction. Also the STM simulations do not correspond well with the experimental observation.

Table 4.3: *Maximal simulated current above the* 2×1-r *and the* $\sqrt{3} \times \sqrt{3}$ *reconstructions.*

Reconstruction	Highest atom [Å] (0 is arbitrary)	Maximal current [μA]
2×1-r	3.4	3.3
vacancy	2.3	0.8
adatom	4.5	15.2
buckled (1)	3.6	1.4
Pandey like	3.6	2.8

Note: The height of the tip was 7.6 Å above arbitrary 0.
The applied bias voltage was + 1.5 V.

The *vacancy* reconstruction can be expelled from the list of suitable candidates for the observed $\sqrt{3} \times \sqrt{3}$ reconstruction, due to its energetic unfavourableness and disagreement between STM simulations and the experiments.

The STM simulations of the *buckled* reconstruction fits to the experiment quite well (see figure 4.19 **(a)**) and the maximal current simulated above the *buckled* reconstruction is slightly lower, than the maximal current simulated above *2×1-r*. This is also in good agreement with measured line profile. However, according to the dynamic simulations and the total energy calculations the most probable would be the continuous *Pandey like* → *buckled* → *Pandey like* swithing at room temperature. During this transition the *Pandey like* reconstruction would probably change its isomerization, how it was observed in the dynamic simulations. The STM simulations of the *Pandey like* reconstruction at room temperature, which are in good agreement with the experiment, too, also support this option (see figure 4.19 **(b)**). The maximal current simulated above the *Pandey like* reconstruction is bigger than in the the case of the *buckled* reconstruction, but it is still lower than the maximal current simulated above *2×1-r*.

The energetic favourableness of the *buckled* and the *Pandey like* reconstruction is lower than the favourableness of the 2×1 *Pandey chain*. This might support

the fact that after heating of the surface up to the temperature 600 °C all the surface is 2×1 *Pandey chain* reconstructed. On the other hand it does not clarify why the $\sqrt{3} \times \sqrt{3}$ reconstruction grown on the surface. The thorough analysis of obtained experimental STM maps pointed out that $\sqrt{3} \times \sqrt{3}$ reconstructed areas have always some dark spots inside the area. Those dark spots could be vacancies, that can stabilize the *buckled* or the *Pandey like* reconstruction according to the calculations of F. Ancilotto et al. [33].

To sum up all these facts, the dynamical *Pandey like* → *buckled* → *Pandey like* swithing is highly probable the $\sqrt{3} \times \sqrt{3}$ reconstruction observed in the experiment.

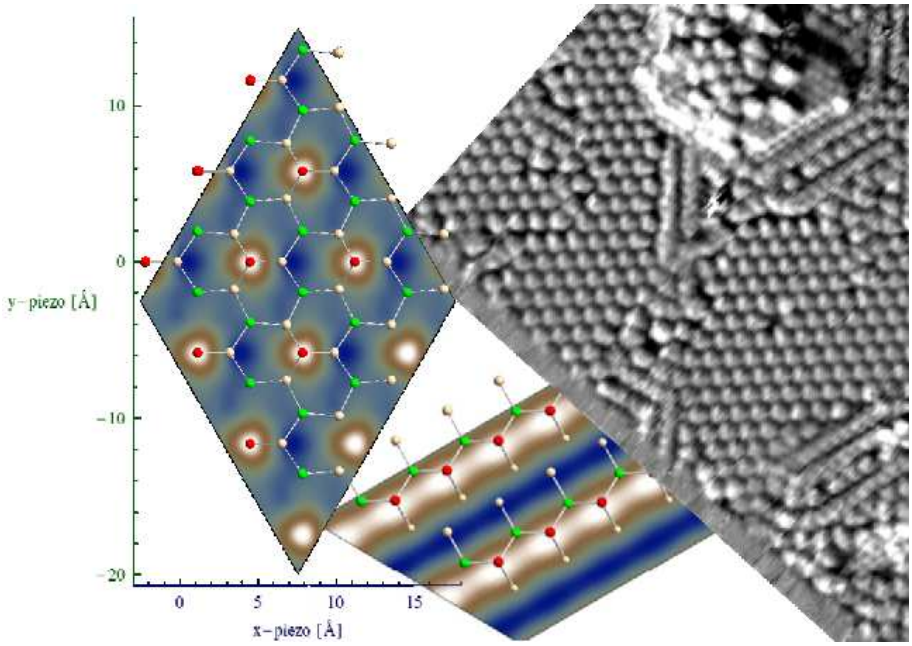

(a)

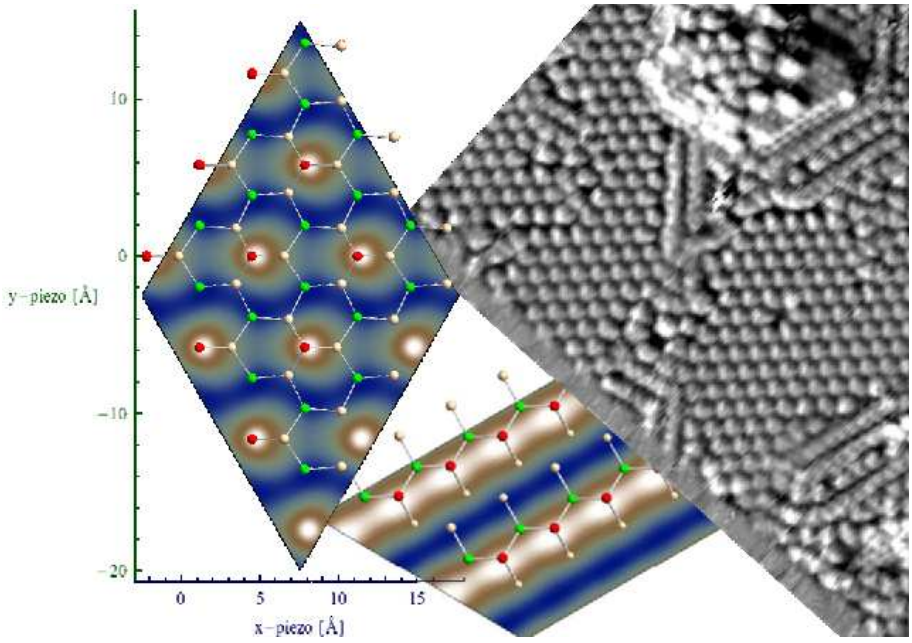

(b)

Figure 4.19: *The comparison of the experimental STM map (right) with simulations of* buckled *reconstruction* **(a)** *and RT simulations of* Pandey like *reconstructed surface* **(b)**. *The experimental STM map was obtained with applied bias voltage + 2.0 in the quasi constant height mode. The simulations were made at constant height mode (4* Å*) above reconstructions with applied bias voltage +1.8 V. For better comparison the STM simulations of* 2×1-r*are shown in the bottom. The simulated and experimental figures have different ratio.*

4.3.2.5 The 7×7 DAS

The properties of the clean 7×7 reconstruction were studied in order to compare them with the properties of the 7×7 reconstruction with the chemisorbed benzene molecule on it.

The resulting geometry of the 7×7 reconstruction is shown on the figure 2.10 and the main results are summarized in the table 4.4. This table shows, that a single adatom of the $\sqrt{3}\times\sqrt{3}$ *adatom* reconstruction is higher above the atoms of the first and the second layer, than the adatoms of the 7×7 reconstruction. The proposed height difference between the adatom and the atom of the second layer by S. D. Solares et al. [32] is 2.50 Å. But S. D. Solares et al. did not specify the position of the adatom in the 7×7 cell. The values obtained from my calculations are around their proposed value (see table 4.4). The length of the bond between the dimer's atoms in my calculations ranges from 2.42 Å to 2.44 Å depending upon the site. According to the calculations of S. D. Solares et al. the bond length between dimer atoms ranges from 2.43 Å to 2.46 Å. The longer bonds in the results of calculations of S. D. Solares et al. are in agreement with their calculated ideal length of Si-Si bond in the bulk, that is 2.35 Å in calculations of S. D. Solares et al., in contrast to 2.30 Å in my calculations. The ideal bond length is influenced primarily by used basis set and also by used *exchange-correlation functional*. S. D. Solares et al. used the basis set of the gaussian functions and The GGA functional PBE [32].

Table 4.4: *The geometrical position of the adatoms and the restatoms in the 7×7 reconstruction: The height of the adatoms and the restatoms above the hole atom of the 7×7 reconstruction - z. The height difference between the adatom and the atom of the first layer (or the second layer in the case of the restatom) - dz_1 - and between the adatom and the atom of the second layer - dz_2.*

Atom	z [Å]	dz_1 [Å]	dz_2 [Å]
fc adatom	3.86	1.31	2.52
fe adatom	3.79	1.29	2.48
uc adatom	3.74	1.30	2.48
ue adatom	3.71	1.26	2.45
fr restatom	3.12	1.15	-
ur restatom	3.18	1.21	-
$\sqrt{3}\times\sqrt{3}$ adatom	-	1.45	2.66

The density of states of the adatoms and the restatoms (see figure 4.20) are in good agreement with the measured dI/dV spectras by M. Švec et al. [37] (see figure 2.12). The PDOS (figure 4.20 **(a)** and **(b)**) shows us that the adatoms have states on the Fermi level, however the dangling bond on the restatom is saturated by charge transfer of an electron from up atoms. So the restatoms have no states on the Fermi level. The density of states together with the geometry give us the first guess how the STM simulations could look like. Because the adatoms are

about 0.6 Å higher then the restatoms and because the adatoms have states on the Fermi level, they are the brightest in the STM figures. However, the restatoms can be very barely seen in the STM maps at all bias voltages. The restatoms can be observed only at the high negative bias voltages, but they are less bright than the adatoms. In the filed states the DOS of the adatoms does not differ so much, therefore the height of the adatoms determines their brightness in the STM figures. Thus, in negative bias voltages the *fc* adatoms are the brightest and the *fe* adatoms are the least bright. On the other hand, in the empty states the DOS compensates the height difference, which means, that all the adatoms are equally bright in the STM maps obtained with positive applied bias voltages. The STM simulations of mine, are shown at the figure 4.21 and they fulfil all the mentioned properties quite well. They are in very good agreement with the experiment (figure 2.11), too.

The graphical representation of the PDOS (figure 4.20 **(c)**) should correspond with dI/dV of the clean 7×7 reconstruction as seen in the figure 4.4 and 2.11 according to eq. (3.7). As you can see in this graphical representation the atoms with highest DOS at the energy - 0.9 eV bellow the Fermi level are the restatoms. The adatom has no states located on them at this energy. Thus, the PDOS is in very good agreement with the measured experimental data.

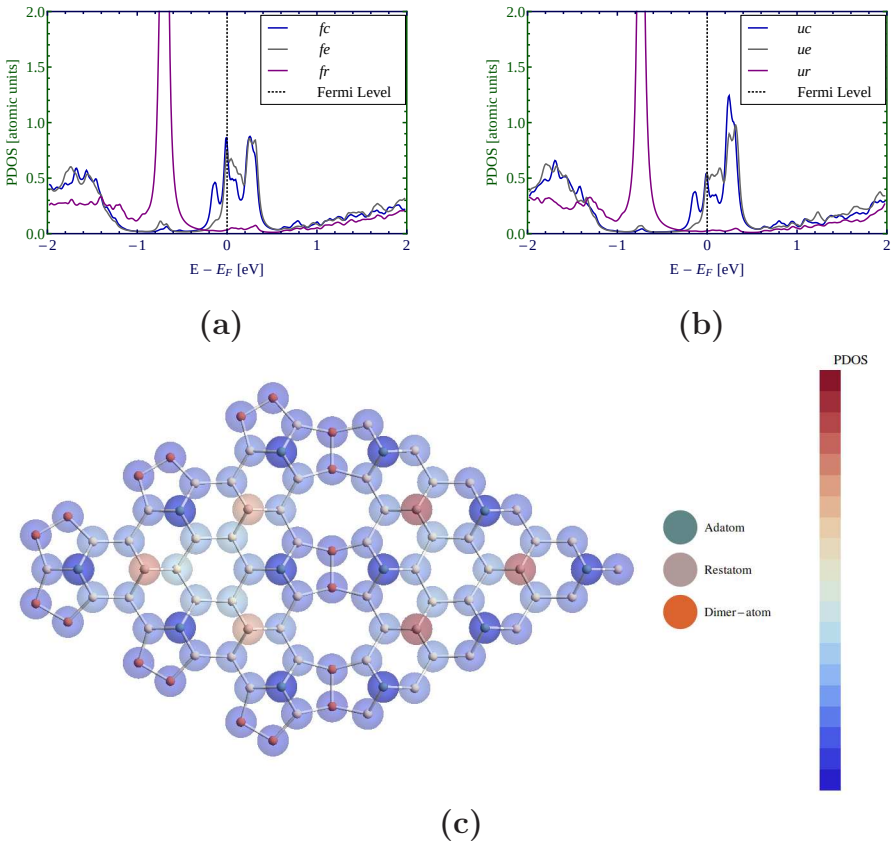

Figure 4.20: *PDOS of the most important atoms of the 7×7 reconstruction:* **(a)** *PDOS of the faulted corner adatom - fc; the faulted edge adatom - fe - and the faulted restatom - fr.* **(b)** *PDOS of the unfaulted corner adatom - uc; the unfaulted edge adatom - ue - and the unfaulted restatom - ur.* **(c)** *Graphical representation of the PDOS of the topmost atoms of the 7×7 at energy - 0.9 eV below the Fermi Level. The dark blue bubbles around the atoms mean, that no states are located on the atoms, while the red bubbles represent a maximal density.*

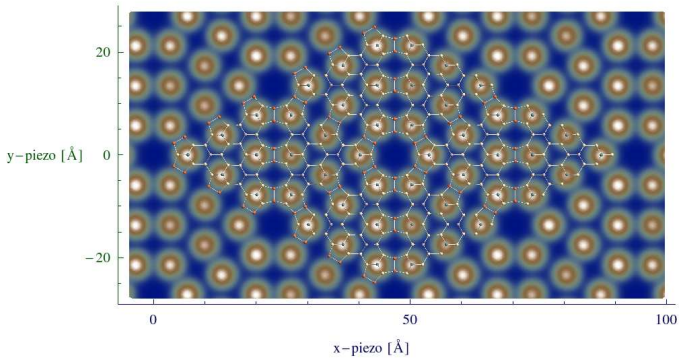

(a)

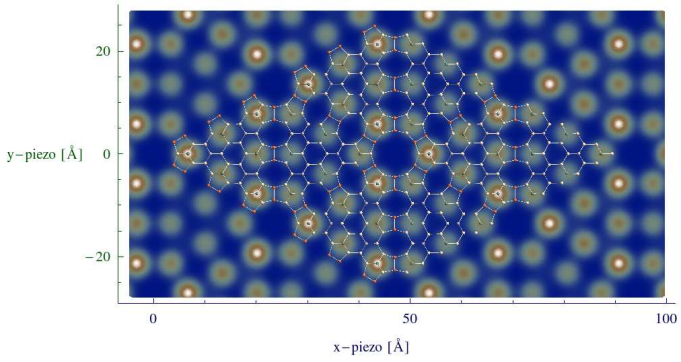

(b)

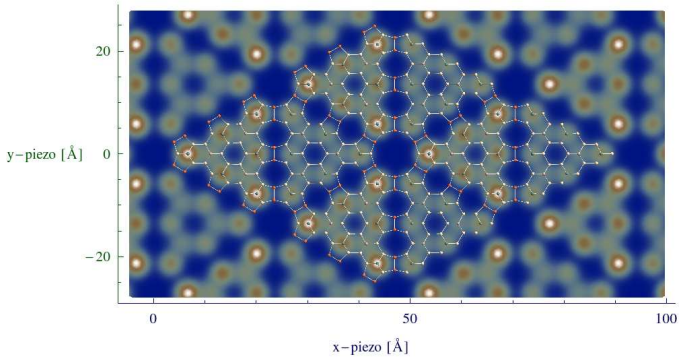

(c)

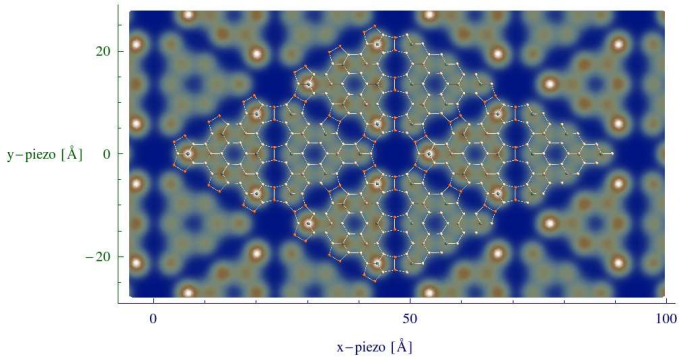

(d)

Figure 4.21: *The STM constant height (5 Å) simulation of 7×7 reconstruction for bias voltage + 0.5 V*: **(a)**; *bias voltage - 0.5 V:* **(b)**; *bias voltage - 1.0 V:* **(c)** *bias voltage - 1.5 V:* **(d)**.

4.3.3 The benzene molecule on the 7×7 DAS

In this chapter I will show the results of the calculations concerning the chemisorption of the benzene molecule on the 7×7 reconstruction in the di-*sigma*-bridge position. The obtained adsorption energies - 2.21 eV or 2.15 eV if the benzene molecule is chemisorbed in the faulted or the unfaulted half unit cell respectively - is far away from the desorption energies obtained from the TDS - $\sim$ 0.96 eV [40], due to the basis set super position error [58] in my calculations.

The chemisorption of the benzene molecule changes not only the geometry of the molecule (the transition: benzene $\rightarrow$ 1,4-cyclohexadien), it also affect the geometry of the atoms to which is the benzene molecule bound. The adatoms nearest to the adsorbed molecule are influenced, too. The adatom to which is bound the benzene molecule always moves upward during the adsorption, however the bound restatom is shifted downward. The nearest adatom also moves upwards, that makes them brighter in the STM maps in the negative bias voltages (this feature will be discussed later). The positions of other atoms are almost intact by the adsorption. The bound adatom is shifted 0.08 Å, 0.15 Å, 0.17 Å and 0.19 Å upward in the case of *b-fc*, *b-fe*, *b-uc* and *b-ue* adsorption respectively. The bound restatoms change their position 0.48 Å, 0.48 Å, 0.52 Å and 0.50 Å downward in the case of *b-fc*, *b-fe*, *b-uc* and *b-ue* adsorption respectively. If the benzene molecule chemisorbs in the *b-fc* position then the nearest adatoms - *fe* adatoms - move 0.15 Å up. If the benzene molecule is in the *b-fe* position then the nearest *fc* adatom is shifted 0.18 Å upward and the *fe* adatom moves 0.11 Å upward. In the case of *b-uc* chemisorption the nearest *ue* adatoms are shifted 0.11 Å upward. When the benzene molecule is in the *b-ue* position then nearest the *uc* adatom moves 0.11 Å up and the *ue* adatom moves 0.10 Å upward.

Together with the changes in the geometry of the 7×7 reconstruction, also the differences in the electronic structure of the 7×7 with chemisorbed benzene can be found. These changes for all the calculated benzene positions are shown in the PDOS in the figure 4.22. The adatoms, which have bond with carbon atom, lose the states on the Fermi level located on these adatoms. That means, the adatoms disappear from the STM maps in all voltages as you can see in the experimental maps (figure 4.5) and the simulated maps (figures 4.23 and 4.24). The states around - 0.7 eV bellow the Fermi level located on the restatoms that bind to the benzene molecule are eliminated, too. So these restatoms disappear from the dI/dV maps (see picture 4.4); it is shown in the graphical representation of the PDOS, too (figure 4.25). The one electron that came onto the restatoms from the adatoms is transfered primarily onto the adatoms nearest to the adsorbed benzene molecule. This charge transfer causes more states on these adatoms and the upward shift of these adatoms mentioned above. Therefore the adatoms nearest to the benzene molecule are brighter in the STM maps in the negative bias voltages. If the adatoms binds to the edge (center) adatom, then the nearest edge adatom in the neighbouring half unit cell loses almost all states bellow the Fermi level. Thus they are less bright in the STM maps than the other edge adatoms in the neighbouring half cell, as you can see in the experimental observations (figure 4.5) as well as in the simulations (figures 4.23 and 4.24).

In the positive bias voltages (empty states) are all the adatoms equally bright, except the adatoms that are bound to the benzene molecule, in the STM experiment (figure 4.5) and almost equally bright in the simulations (figure 4.5). In the

empty states the DOS compensates the height differences between the adatoms as in the case of the clean 7×7, except the adatom bounded to the benzene molecule. The small differences between the experimental and the simulated STM maps can be caused by the absence of the thermal motion of atoms in the simulations or it can be caused by the used approximations in the DFT calculations.

Although, the theoretical simulations correspond to the experimental observations very well, there is a possibility that the adsorbed benzene molecule can be mistaken for an adsorbed hydrogen atom on the adatom or an vacant adatom. The adsorbed hydrogens on the adatoms were observed by means of STM by S. Bulavenko et al. Their results showed, that the hydrogen chemisorbed on the adatom is only the metastable position (the most stable position is the chemisorption on the restatom), but the barrier for the transfer of the hydrogen from the adatom to the restatom is about 0.15 eV, thus the hydrogen remains on the adatom enough long time, so it can be observed in the STM maps. In the STM maps of S. Bulavenko et al. the hydrogen atom adsorbed on the adatom is indicated by disappearance of the adatom in the STM pictures in all bias voltages. On the other hand, other adatoms were not affected by the adsorption [51]. I did the calculations of the hydrogen adsorbed on the *fc* adatom and *uc* adatom. I leave out the positions of the hydrogen on the edge atoms, because the calculations are very time consuming and because I did not expect that this adsorption would significantly differ from the cases I studied. My results are in very good agreement with the mentioned experiment of S. Bulavenko et al. The dangling bond on the adatom is fully saturated by the adsorption of the hydrogen, while the other atoms are intact by the adsorption. The STM simulation of the hydrogen adsorbed on the *fc* adatom is shown in the figure 4.26 **(a)**. The STM simulation for the hydrogen adsorbed on the *uc* adatom look the same, except that in this simulation disappears the *uc* adatom. Therefore the hydrogen adsorbed on the adatom can be distinguished from the adsorbed benzene molecule by brightness of the adatoms nearest to the disappeared adatom in the STM maps obtained with negative bias voltages.

The vacant adatom in the 7×7 cell was studied experimentally and theoretically by L. Chen et al. [52]. Their STM experiment showed, that the vacant adatom in 7×7 behaves similarly as the adsorbed benzene molecule on the 7×7. That means, that the adatoms nearest to the vacancy are brighter in the negative bias voltages. The vacant adatom also causes that the peak in the PDOS at $\sim$ - 0.8 eV bellow the Fermi Level moves onto the energy $\sim$ - 0.5 eV bellow the Fermi level. Thus the restatom disappears from the dI/dV maps obtained at bias voltages around - 1 V [52]. My calculations of the vacant *fc* adatom and the vacant *uc* adatom in the 7×7 reconstructions are in quite good agreement with calculations of PDOS performed by Chen et al. The PDOS of the restatom nearest to the vacant adatom is in the picture 4.27. But on the other hand my STM simulations do not show the adatoms nearest to the vacant atom more bright than the other adatoms in the unimpaired 7×7 reconstruction (figure 4.26. This can be caused by the used tungsten tip in the simulations or by the already mentioned thermal motion.

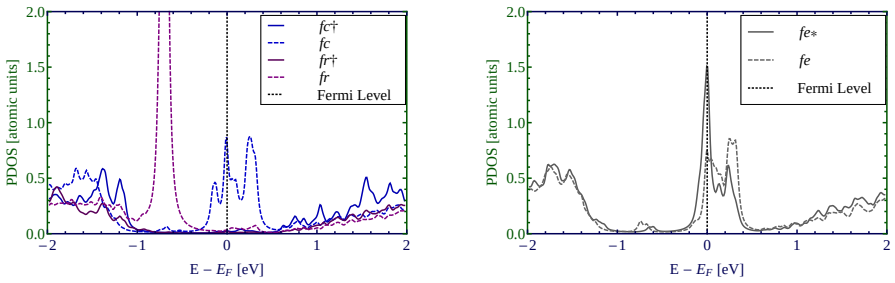

(a)

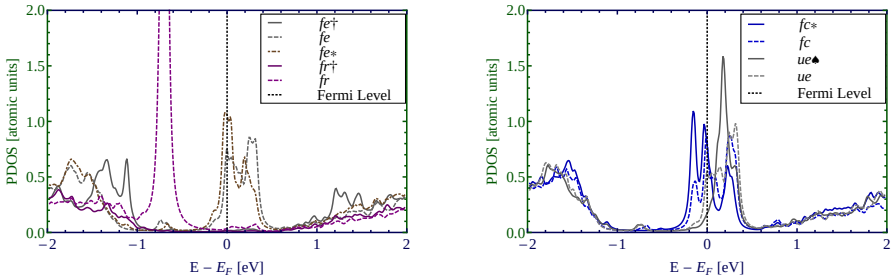

(b)

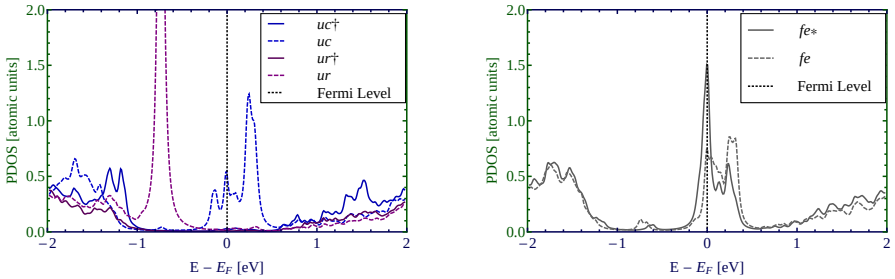

(c)

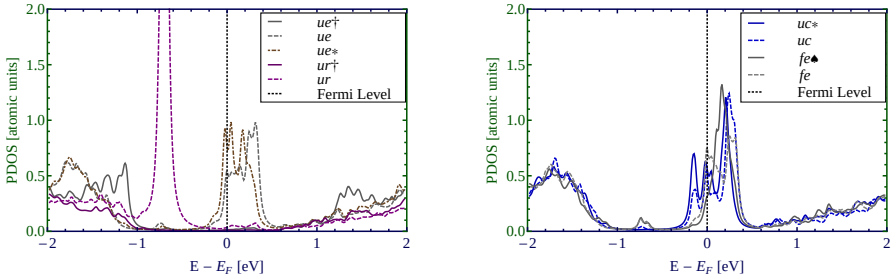

(d)

Figure 4.22: *PDOS of the most important atoms of the 7×7 reconstruction with the chemisorbed benzene molecules on it in comparison with the PDOS of the atoms of the clean 7×7 (dashed lines):* **(a)** *PDOS for the* b-fc *chemisorption;* **(b)** *PDOS for the* b-fe *chemisorptio;* **(c)** *PDOS for the* b-uc *chemisorption.* **(d)** *PDOS for the* b-ue *chemisorption. The* † *marks the atoms that are bound to the benzene molecule. The adatom nearest to the adsorbed molecules are labeled* ∗*. If the benzene molecule binds with any edge adatom, then the PDOS of the nearest edge adatom in the neighbouring half unit cell is also changed. This atoms are labeled* ♠*.*

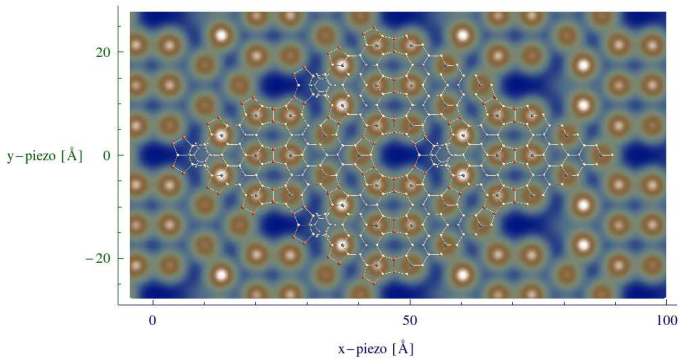

(a)

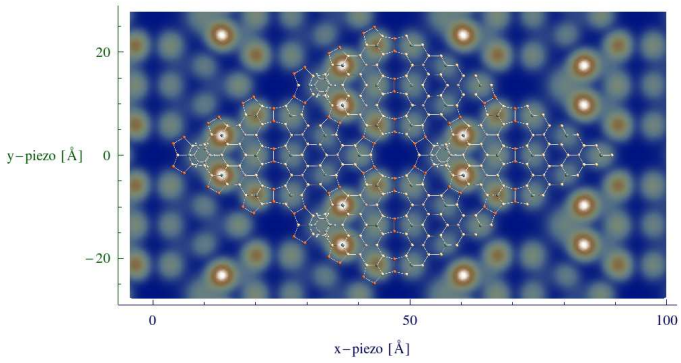

(b)

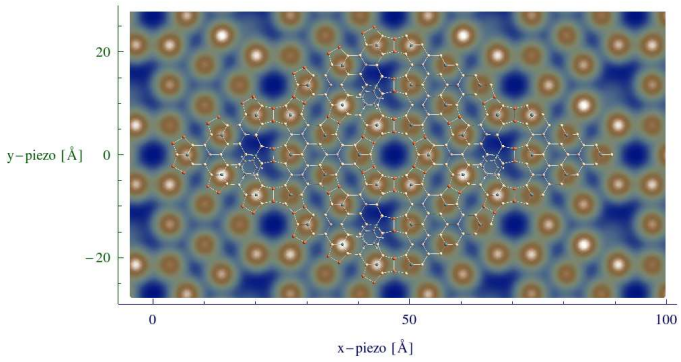

(c)

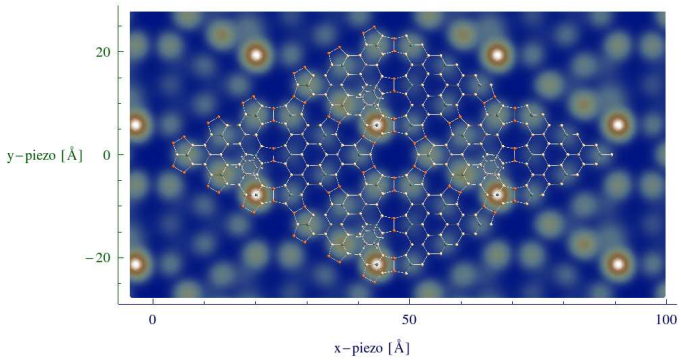

(d)

Figure 4.23: *The STM constant height (5 Å) simulation of the benzene adsorbed on 7×7 for bias voltage + 0.5 V (left column) and bias voltage - 0.5 V (right column). The benzenes are adsorbed in different positions*: **(a)** *Benzene in position b-fc, bias voltage + 0.5 V;* **(b)** *Benzene in position b-fc, bias voltage - 0.5 V;* **(c)** *Benzene in position b-fe, bias voltage + 0.5 V;* **(d)** *Benzene in position b-fe, bias voltage - 0.5 V.*

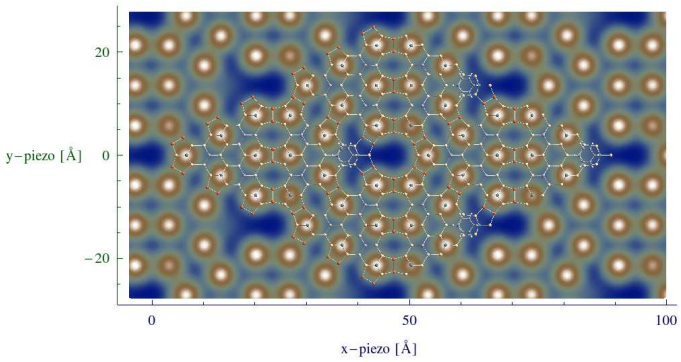

(a)

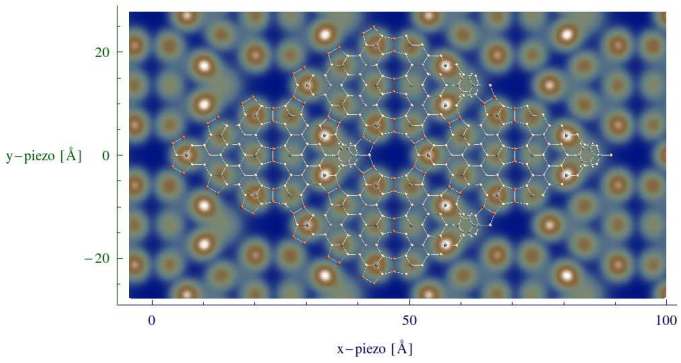

(b)

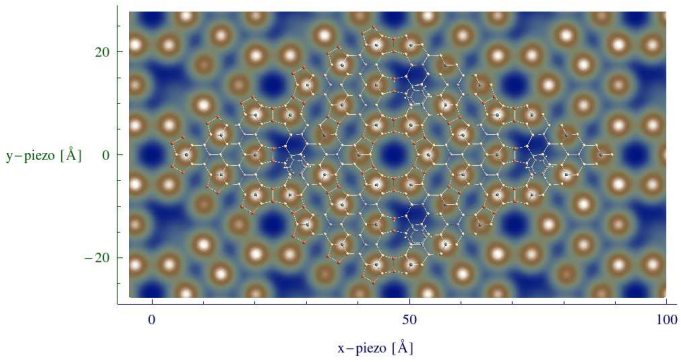

(c)

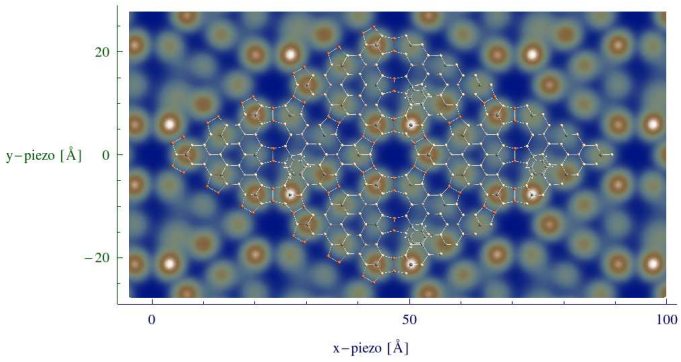

(d)

Figure 4.24: *The STM constant height (5 Å) simulation of the benzene adsorbed on 7×7 for bias voltage + 0.5 V (left column) and bias voltage - 0.5 V (right column). The benzenes are adsorbed in different positions*: **(a)** *Benzene in position b-uc, bias voltage + 0.5 V;* **(b)** *Benzene in position b-uc, bias voltage - 0.5 V;* **(c)** *Benzene in position b-ue, bias voltage + 0.5 V;* **(d)** *Benzene in position b-ue, bias voltage - 0.5 V.*

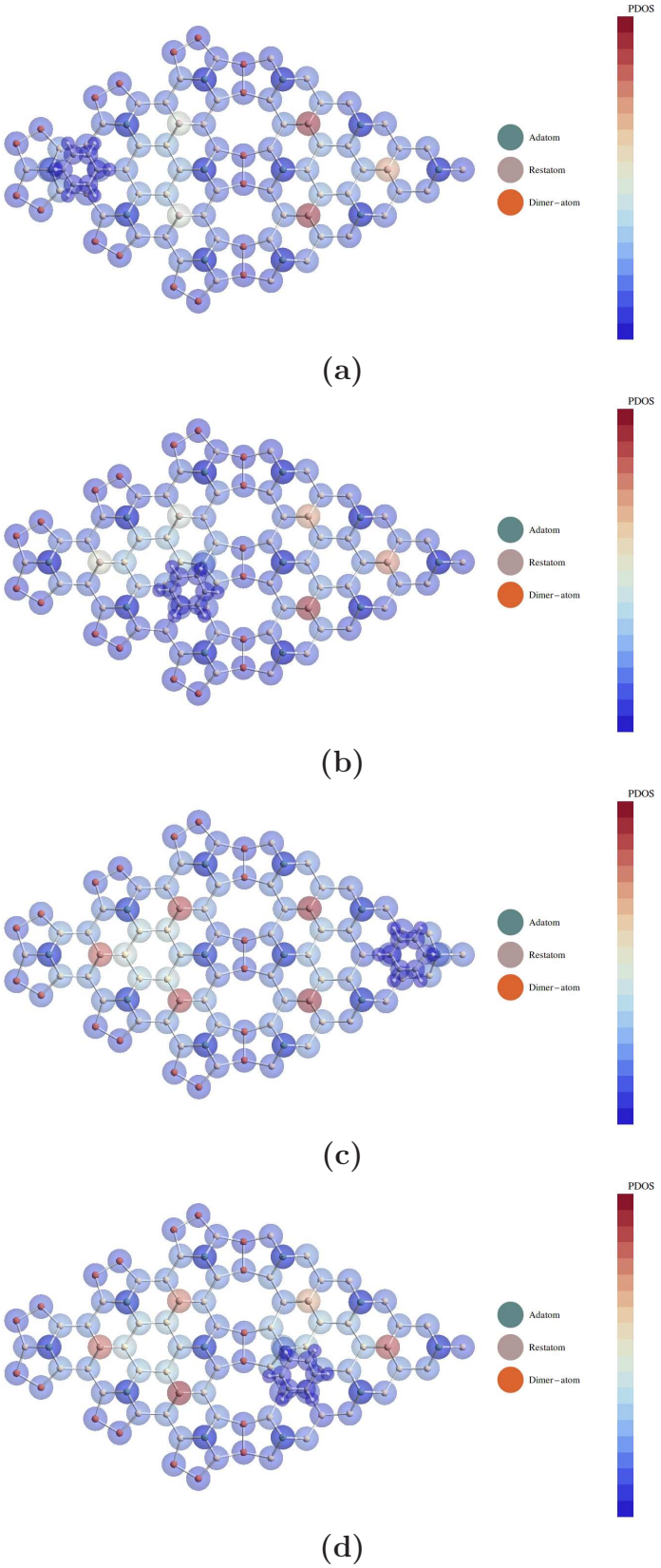

Figure 4.25: *Graphical representation of PDOS of the topmost atoms for different structures at the energy - 0.9 eV below Fermi Level.*: **(a)** *b-fc* ; **(b)** *b-fe* ; **(c)** *b-uc* ; **(d)** *b-ue. The dark blue bubbles around the atoms mean, that no states are located on the atoms, while the red bubbles represent a maximal density.*

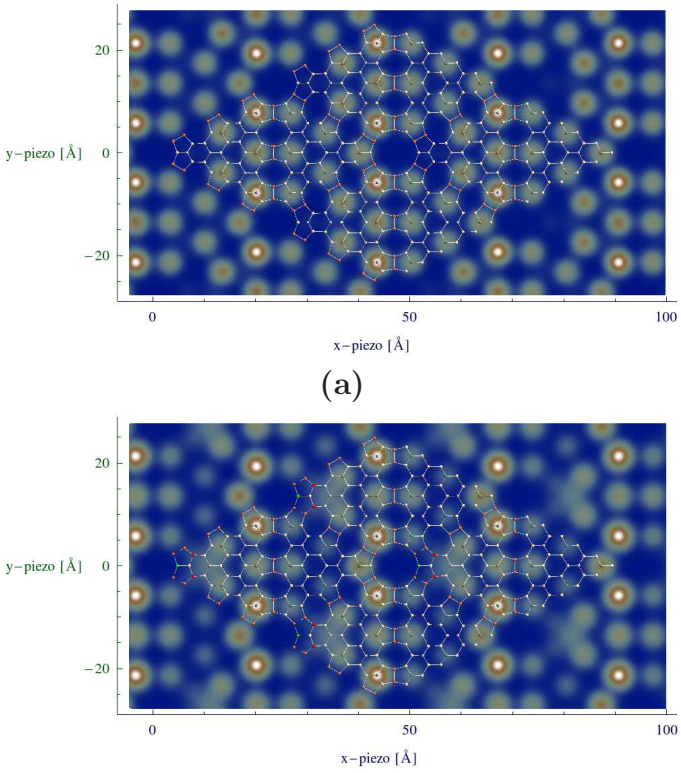

Figure 4.26: *The constant height (5 Å) STM simulations of*: **(a)** *H adsorbed on the fc adatom*; **(b)** *The 7×7 with the vacant fc adatom. The backbone atoms are buckled. Two up backbone atoms are represented red, one down backbone atom is represented green in the model shown in the STM simulation.*

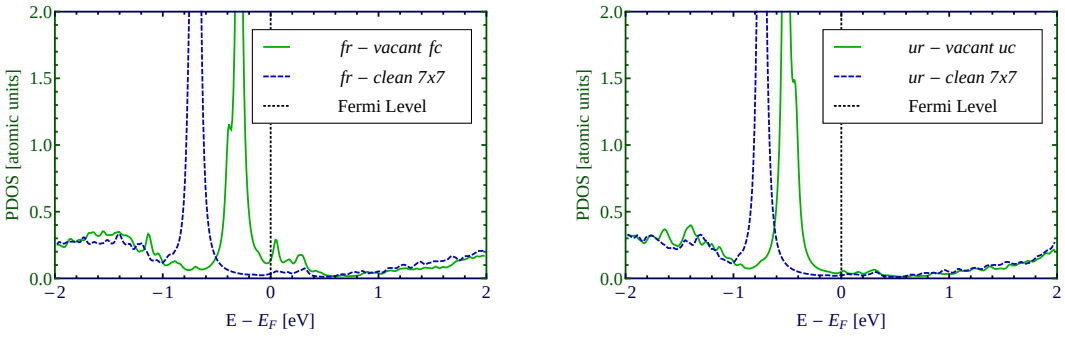

Figure 4.27: **(a)** *The PDOS of the nearest fr restatom to the fc vacant adatom in comparison with the PDOS of the restatom of the clean 7×7.***(b)** *The PDOS of the nearest ur restatom to the uc vacant adatom in comparison with the PDOS of the restatom of the clean 7×7.*.

The STM maps from the experiment and the simulations of the adsorbed benzene or the adsorbed hydrogen on the adatom or the vacant adatom do not differ from each other. They only show the dissapeared adatom, while the others adatoms are equally bright [51, 52].

To make sure, that the observed features in our experiment are really related to the chemisorbed benzene molecule I performed the STM simulation of the height profiles of the clean 7×7, the 7×7 with chemisorbed benzene in all studied positions, the 7×7 with chemisorbed hydrogen in all studied positions and the 7×7 with vacant *fc* or *uc* adatom. These height profiles are compared with the height profiles obtained from the experiment on the figures 4.28 and 4.29. The adsorbed benzene molecule can be differentiated from the vacancy by the height of the line profiles obtained above the adatoms nearest to the adsorption or the vacancy. This height of the line profile is higher in the case of the adsorbed benzene, than in the case of vacancy or the adsorbed hydrogen. As you can see on these figures (4.28, 4.29)the simulated height profiles of the 7×7 with the chemisorbed benzene molecule are in excellent agreement with the simulated curves. Thus, the observed features in the experiment of Prof. Alastair Mclean shown on the figure 4.5,are almost certainly related to the chemisorbed benzene.

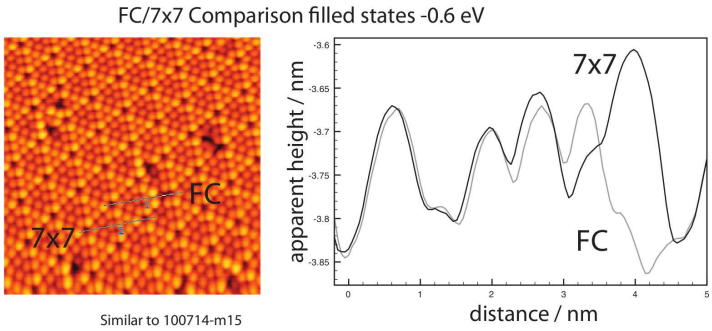

(a)

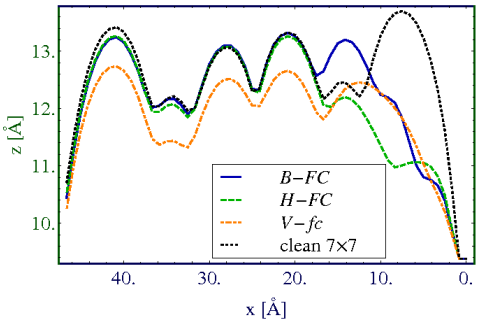

(b)

Figure 4.28: *The constant current STM height profiles of the benzene molecule adsorbed in the b-fc position*: **(a)** - *The height profile obtained from the experiment;* **(b)** - *The simulated height profile. The starting point for the simulation was directly above the hole atom with height 5 Å above the adatoms. O is arbitrary in the z-scale in the simulation and in the experiment. The lineprofiles are compared with the clean 7×7 reconstruction, with the hydrogen adsorbed on the fc adatom and with the 7×7 with vacant fc adatom.*

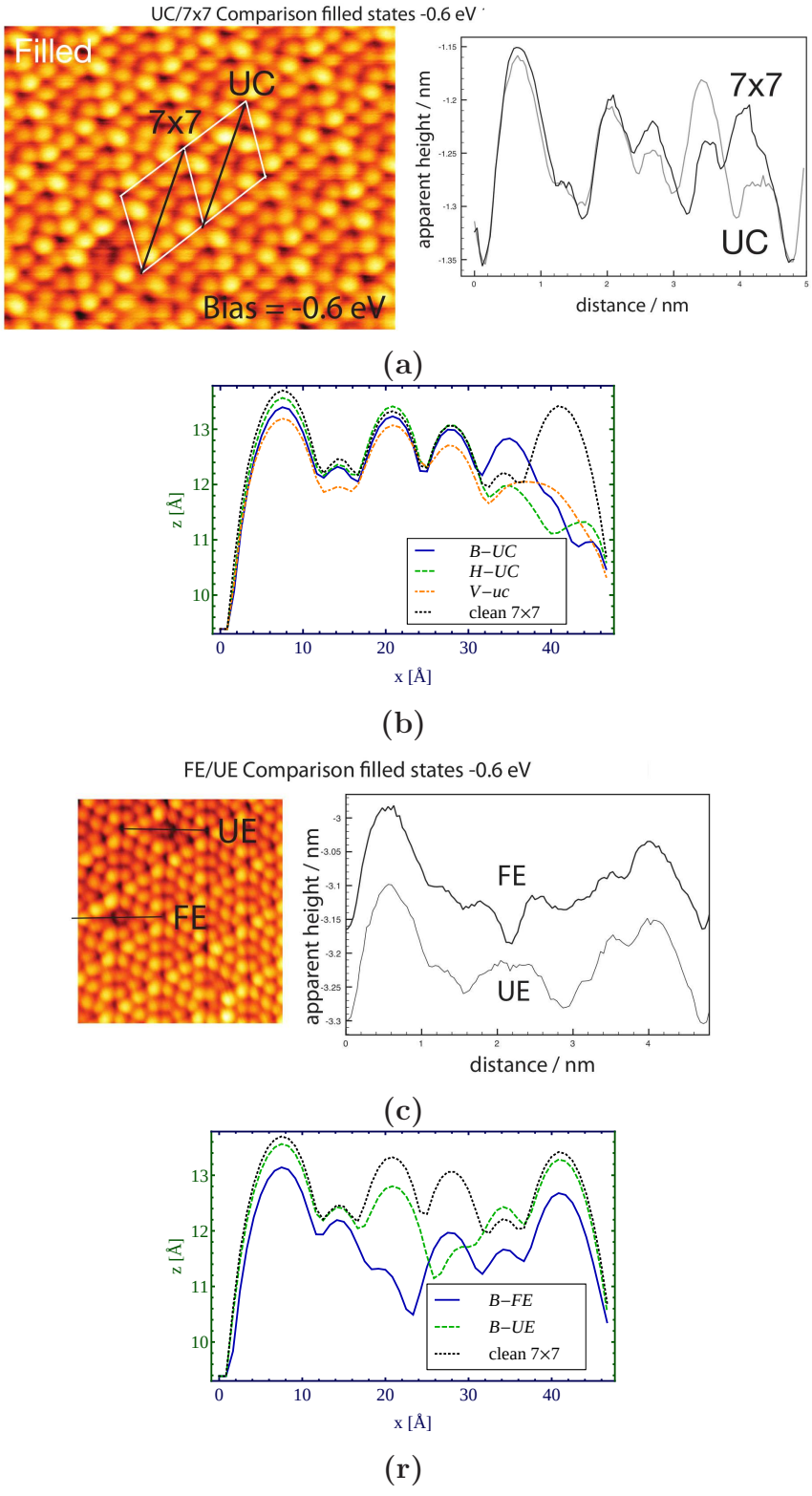

Figure 4.29: *The constant current STM height profiles of the benzene molecule adsorbed in the positions:* **(a),(b)** *- b-uc,* **(c,d)** *- b-fe and b-ue.* **(a),(c)** *- The height profile obtained from the experiment;* **(b,d)** *- The simulated height profile. The starting point for the simulation was directly above the hole atom with height 5 Å above the adatoms. O is arbitrary in the z-scale in the simulations and in the experimental profiles. The height profiles of the b-ucadsorption are compared with the clean 7×7 reconstruction, with the hydrogen adsorbed on the uc adatom and with the 7×7 with vacant fc adatom.*

Conclusion

In my diploma thesis I concerned the theoretical calculations of the atomic and the electronic structure of the reconstructions of the Si (111) surface and the interaction of this surface with an adsorbate. The calculations followed up the experimental STM measurement in which an unknown $\sqrt{3}\times\sqrt{3}\ R30°$ reconstruction of Si (111) surface was observed and the STM experiment that examined the chemisorbed benzene molecule on the 7×7 reconstructed Si (111) surface at room temperature.

In the first part I did DFT-LDA calculations with the Fireball code, in order to compare energetic favourableness of several different reconstructions of the Si (111) surface. These calculations reproduced the known fact, that the most stable reconstruction is the 7×7 DAS reconstruction. The DFT results together with the following STM simulations performed by means of the STM code, found appropriate candidate on the observed $\sqrt{3}\times\sqrt{3}$ reconstruction in the first mentioned experiment. This candidate was the reconstruction, whose topmost atoms are buckled - one is the up atom, two are the down atoms.

However, the dynamic simulations at room temperature result into more favourable reconstruction, which I call the *Pandey like*. This reconstruction is formed by rebonding of the *buckled* reconstruction. The following dynamic simulations have showed that the *Pandey like* reconstruction would change its isomerization at room temperature. The STM simulation concerning the changes of isomerisation are in good agreement with the experimental STM maps. Thus, the highly probable model of observed $\sqrt{3}\times\sqrt{3}$ reconstruction was found.

The STM maps of the 7×7 with the adsorbed benzene molecule on it, reproduced the features published in the literature. The simultaneously measured dI/dV maps, which were performed for the first time for this system, shown the evidence of the carbon-restatom bond.

I calculated the atomic and the electronic structure of the 7×7 reconstruction with the benzene molecule adsorbed in the so called di-σ-bridge position, when the benzene molecule binds to the adatom and the restatom of the 7×7. The changes in the structures caused by the chemisorption of the benzene molecule indicated that the features observed in the STM and the dI/dV match with the calculated models. The simulations of the STM maps and the line profiles excellently agree with the experiment. So the experiment together with the DFT calculations proved that the benzene molecule chemisorbs in the di-σ-bridge positions at room temperature on the 7×7 DAS. The DFT calculations also suggest how to distinguish the adsorbed benzene molecule from adsorbed hydrogen on the adatom or from vacant adatom.

Bibliography

[1] W. Koch, M. C. Holthausen , *A Chemist Guide to Density Functional Theory*. 2nd ed. Germany: Willey-VCH, 2001. ISBN 3-527-60004-3.

[2] Ch. J. Cramer , *Essentials of Computional Chemistry: Theories and Models*. 2nd. ed. Great Britain: Willey-VCH, 2004. ISBN 0-470-09182-7.

[3] W. Yang, R. G. Parr , *Density-Functional Theory of Atoms and Molecules.* 1st. ed. USA, Oxford University Press, 1989 ISBN 0-19-504279-4

[4] O. Krejčí , *Theoretical calculation of stability and electronic structure of Si surface.* Bc. Thesis, Faculty of Physics, Charles University in Prague.

[5] D. M. Ceperley, B. J. Alder , *Ground State of the Electron Gas by a Stochastic Method*. Phys. Rev. Lett. 45, 566–569 (1980)

[6] N. Yakovin, P. A. Dowben , *The Problem of the Band Gap in LDA Calculations*. Surface Review and Letters, Vol. 14, No. 3 (2007) 481–487

[7] A. D. Becke , *Density-functional exchange-energy approximation with correct asymptotic behavior,* Phys. Rev. A 38, 3098–3100 (1988)

[8] John P. Perdew and Yue Wang , *Accurate and simple analytic representation of the electron-gas correlation energy,* Phys. Rev. Lett. 77, 3865–3868 (1996)

[9] John P. Perdew, Kieron Burke, and Matthias Ernzerhof , *Generalized Gradient Approximation Made Simple,* Phys. Rev. B 45, 13244–13249 (1992)

[10] Chengteh Lee, Weitao Yang, and Robert G. Parr , *Development of the Colle-Salvetti correlation-energy formula into a functional of the electron density,* Phys. Rev. B 37, 785–789 (1988)

[11] R. Dronskowski , *Computional Chemistry of Solid State Materials*. 1st. ed. Germany: Willey-VCH, 2005. ISBN 3-527-31410-5

[12] R. M. Martn , *Electronic Structure: Basic Theory and Practical Methods.* 2nd. ed. The United Kingdom: Cambridge University Press, 2005. ISBN 0-521-78285-6

[13] N. W. Ashcroft, N. D. Mermin , *Solid State Physics.* 2nd ed. USA: Thomson-Learing, 1976. ISBN 0-03-083993-9.

[14] P. Hofmann , *Solid State Physics: An Introduction.* 1st ed. Germany: Willey-VCH, 2008.

[15] wwww.fireball-dft.org

[16] D. R. Hamman, M. Schülter, C. Chiang , *Norm-Conserving Pseudopotentials*. Phys. Rev. Lett. 43. 1494-1497 (1979).

[17] J. P. Lewis,P. Jelínek, J. Ortega,A. A. Demkov, D. G. Trabada, B. Haycock, H. Wang, G. Adams, J. K. Tomfohr, E. Abad, H. Wang, D. A. Drabold ,*Advances and applications in the FIREBALL ab initio tight-binding molecular-dynamics formalism* Physica Status Solidi (B) Basic Research Volume 248, Issue 9, September 2011, Pages 1989-2007

[18] P. Jelínek, H. Wang, J. P. Lewis, O. F. Sankey, J. Ortega , *Multi-center aproach to the exchange/correlation interactions in ab initio tight-binding methods,* Phys. Rev. B. 71.(2005) 235101.

[19] J.P. Perdew and A. Zunger , *Self-interaction correction to density-functional approximations for many-electron systems* Phys. Rev. B 23, 5048–5079 (1981).

[20] D.M. Ceperley and B.J Alder , *Ground State of the Electron Gas by a Stochastic Method* Phys. Rev. Lett. 45, 566–569 (1980).

[21] Otto F. Sankey and David J. Niklewski , *Ab initio multicenter tight-binding model for molecular-dynamics simulations and other applications in covalent systems,* Phys. Rev. B 40, 3979–3995 (1989).

[22] A. Zangwill , *Physics at Surfaces*. 1st. ed. USA: Cambridge University Press, 1988. ISBN 0-521-34752-1

[23] M. Lannoo, P. Friedel , *Atomic and Electronic Structure of Surfaces: Theoretical Foundations*. 1st. ed. Germany: Springer-Verlag Berlin Heilderberg, 1991. ISBN 3-540-52682-X

[24] A. A. Stekolnikov, J. Furthmuller, and F. Bechstedt , *Absolute surface energies of group-IV semiconductors: Dependence on orientation and reconstruction,* Phys. Rev. B 65, 115318 (2002).

[25] K. C. Pandey , *New π-Bonded Chain Model for Si(111)-(2×1) Surface,* Phys. Rev. Lett. 47, 1913–1917 (1981)

[26] J. K. Garleff, M. Wenderoth, K. Sauthoff, R. G. Ulbrich and M. Rohlfing , *2×1 reconstructed Si(111) surface: STM experiments versus ab initio calculations,* Phys. Rev. B 70, 245424 (2004).

[27] R. J. Wilson and S. Chiang , *Structure of the Ag/Si(111) surface by scanning tunneling microscopy,* Phys. Rev. Lett. 58, 369–372 (1987).

[28] E. Ganz, F. Xiong, I. Hwang, and J. Golovchenko , *Submonolayer phases of Pb on Si(111),* Phys. Rev. B 43, 7316–7319 (1991).

[29] J. Nogami, Sang-il Park, C.F. Quate ,*An STM study of the gallium induced $\sqrt{3}\times\sqrt{3}$ reconstruction of Si(111),* Surf. Sci. 203, L631–L636 (1988).

[30] W. C. Fan and A. Ignatiev , *Observation and structural determination of $(\sqrt{3}\times\sqrt{3})R30^{\circ}$ reconstruction of the Si(111) surface,* Phys. Rev. Lett. 62, 1516–1519 (1989).

[31] H. Minoda, T. Sato, K. Yagi, Y. Tanishiro, M. Iwatsuki , *Formation of anomalously wide Si(1 1 1) $\sqrt{3} \times \sqrt{3}$ clean surface and its stability,* Surf. Sci., 493, 157-165 (2001).

[32] S. D. Solares, S. Dasgupta, P. A. Schultz,Y. Kim, C. B. Musgrave, W. A. Goddard III , *Density Functional Theory Study of the Geometry, Energetics, and Reconstruction Process of Si(111) Surfaces,* Langmuir 2005, 21, 12404-12414.

[33] F. Ancilotto, A. Selloni, E. Tosatti , *Theory of vacancy-stabilized ($\sqrt{3} \times \sqrt{3}$) displacive reconstruction of the clean Si(111) surface,* Phys. Rev. B 43, 14726 (1991).

[34] K. Takayanagi, Y. Tanishiro, M. Takahashi, and S. Takahashi , *Structural analysis of Si (111)-7×7 by UHV-transmission electron diffraction and microscopy,* J. Vac. Sci. Technol. A 3, 1502 (1985).

[35] M. E. Garah, Y. Makoudi, E. Duverger, F. Palmino, A. Rochefort, and F. Cherioux , *Large-Scale Patterning of Zwitterionic Molecules on a Si(111)-7×7 Surface,* ACS NANO 5, 424–428 (2011).

[36] M. Švec , *Structure and electronic properties of metal-semiconductor interfaces at low coverage,* Ph.D. Thesis, Faculty of Physics, Charles University in Prague.

[37] M. Švec, P. Mutombo, P. Shukrinov, V. Dudr and V. Cháb , *Phase-sensitive lock-in imaging of surface densities of states,* Nanotechnology 17 (2006) 213–216.

[38] W. von Niessen, L. S. Cederbaum, W. P. Kraemer , *The electronic structure of molecules by a many-body approach. I. Ionization potentials and one-electron properties of benzene,* J. Chem. Phys., Vol. 65, No.4 (1976).

[39] K. S. Yong, S. Yang, Y. P. Zhang, P. Wu, and G. Q. Xu, *Adsorption-Induced Desorption of Benzene on Si(111)-7×7 by Substrate-Mediated Electronic Interactions*, Langmuir, 24, 3289-3293 (2008).

[40] Y. Cao, X. M. Wei, W.S Chin, and Y. H. Lai, J. F. Deng, S. L. Bernasek, G. Q. Xu, *Formation of di-sigma bond in benzene chemisorption on Si(111)-7×7*, J. Phys. Chem. B 58, 5698-5702 (1999).

[41] M. Carbone, M. Piancastelli, R. Zanoni and G. Comtet, *A low symmetry adsorption state of benzene on Si(111) 7×7 studied by photoemission and photodesorption*, Surf. Sci. 407, 275–281 (1998).

[42] M. Carbone, M. Piancastelli, M. Casaletto, R. Zanoni, G. Comtet, G. Dujardin and L. Hellner, *Formation of di-sigma bond in benzene chemisorption on Si(111)-7×7*, J. Phys. Chem. B 61, 8531-8536 (2000).

[43] D. E. Brown, D. J. Moffatt and R. A. Wolkow, *Isolation of an intrinsic precursor to molecular chemisorption*, Science 279, 542-544 (1998).

[44] S. Horn and S. Patitsas, *STM study of charge transfer and the role of rest-atoms in the binding of benzene to Si(111)7×7*, Surf. Sci. 602, 630-637 (2008).

[45] R. A. Wolkow, D. J. Moffatt, *The frustrated motion of benzene on the surface of Si(111)*, J. Chem. Phys 103, 10696-10700 (1995).

[46] T. Kawasaki, D. Sakai, H. Kishimoto, A. A. Akbar, T. Ogawa, C. Oshima, *Adsorption and desorption of benzene on Si(111)-7×7 studied by scanning tunnelling microscopy*, Surf. Interface Anal. 31, 126-130 (2001).

[47] Z. H. Wang, Y. Cao and G. Q. Xu, *The binding of benzene on Si(111)-(7×7): a theoretical modelling approach*, Chem. Phys. Lett. 338, 7-13 (2001).

[48] I. D. Petsalakis, J. C. Polanyi, G. Theodorakopoulos, *Theoretical study of the induced attachment of benzene to Si(111)7×7*, Surf. Sci. 544, 162-169 (2003).

[49] H. Tomimoto, *Study of adsorption structure of benzene and toluene on Si(111)7×7 surfaces*, Surf. Sci. 566-568, 664-670 (2004).

[50] I. D. Petsalakis, J. C. Polanyi, G. Theodorakopoulos, *Theoretical study of benzene, toluene, and dibromobenzene at a Si (111)7×7 surface*, Isr. J. Chem. 45, 111-126 (2005).

[51] S.Yu. Bulavenko, P.V. Melnik, M.G. Nakhodkin, A. Goriachko, *Investigation of hydrogen interaction with the Si(111)-7×7 surface by STM with Bi/W tips*, Surf. Sci. 600, 1185–1192 (2006).

[52] L. Chen, B. C. Pan, H. Xiang, B. Wang, J. Yang, J. G. Hou and Q. Zhu, *Observation of local electronic structures of adatom vacancies in Si(111)-7×7 surface in real space*, Phys. Rev. B 75, 085329 (2007).

[53] E. Meyer, H. J. Hug, R. Bennewitz , *Scanning Probe Microscopy: The Lab on a Tip*. 1st ed. Berlin: Springer, 2004. ISBN 3-540-43180-2.

[54] C. J. Chen , *Introduction to Scanning Tunneling Microscopy*. 2nd ed. USA: Oxford University Press, 1993. ISBN 0195071506.

[55] J. M. Blanco, F. Florez, R. Pérez , *STM-theory: Image potential, chemistry and surface relaxation,* Progress in Surface Science 81.(2006) p. 403-443.

[56] Philip B. Lukins, Tom Oates , *Single-molecule high-resolution structure and electron conduction of Photosystem II from scanning tunneling microscopy and spectroscopy,* Biochimica et Biophysica Acta 1409 (1998) 1-11.

[57] Hendrik J. Monkhorst and James D. Pack , *Special points for Brillouin-zone integrations,* Phys. Rev. B 13, 5188-5192 (1976).

[58] R. M. Balabin , *Enthalpy difference between conformations of normal alkanes: Intramolecular basis set superposition error (BSSE) in the case of n-butane and n-hexane,* J. Chem. Phys. 129, 164101 (2008).

List of Tables

List of Abbreviations

b-fc	Benzene molecule bound to the faulted corner adatom
b-fe	Benzene molecule bound to the faulted edge (centre) adatom
b-uc	Benzene molecule bound to the unfaulted corner adatom
b-fc	Benzene molecule bound to the unfaulted edge (centre) adatom
DAS	Dimer-Adatom-Stacking-fault model (7×7 reconstruction)
dI/dV	Spectroscopic operational mode of the STM
DFT	Density Functional Theory.
DOS	Density Of States.
fc	Faulted corner adatom
fe	Faulted edge (centre) adatom
fr	Restatom in the faulted half unit cell
GGA	Generalized Gradient Approximation.
HREELS	High-Resolution Electron Energy Loss Spectroscopy.
LCAO	Linear Combination of Atomic Orbitals.
LDA	Local Density Approximation.
LDOS	Local Density Of States.
LEED	Low-Energy Electron Diffraction.
PDOS	Partial Density Of States.
RT	Room Temperature.
SCF	Self-Consistent Field.
STM	Scanning Tunnelling Microscopy.
TDS	Thermal Desorption Spectroscopy.
uc	unfaulted corner adatom
ue	unfaulted edge (centre) adatom
ur	Restatom in the unfaulted half unit cell